of the Daresbury SRS was used. The sample to detector distance was chosen to cover a scattering vector range from $2 \times 10^{-2} < q < 1.8 \times 10^{-1}$ Å^{-1} and $4 \times 10^{-3} < q < 5 \times 10^{-2}$ Å^{-1} respectively.

In Figure 2 the low angle diffraction pattern is shown for a sample aligned with its axis either parallel to or at right angles to the X-ray beam. The radius of gyration of cross section, R_c, can be calculated from the Guinier approximation [14].

$$I(q) = I(0)e^{-\frac{q^2 R_c^2}{2}}$$

For cylindrical scattering objects, R_c is related to the dimensions of the cylinder according to

$$R_c^2 = \frac{R_{outer}^2 + R_{inner}^2}{2} + \frac{h^2}{12}$$

Experimentally it was determined that this value ranged between 167 - 160 Å. Since the length, h, is, on the scattering range that we're looking at, much too large, it can be assumed that this length will not contribute to the scattering and only the first term remains. If we now take the dimer dimension in the radial direction, i.e. the cylinder wall thickness, to be 65 Å [1] and thus substituting $R_{inner} = R_{outer} - 65$ Å, we can calculate that the external radius is between 170 - 180 Å. These values have been used as the starting parameters in the fitting procedure described below.

Helical diffraction theory [11] tells us that the scattering pattern on the equator of the fibre diffraction pattern can be explained as a combination of a Fourier Transform (FT) of the basic hollow cylinder modulated by cylindrical Bessel functions of the order corresponding with the symmetry in the equatorial plane. This can be approached in two equivalent ways. Either one can use a J_0 Bessel function to describe the cylinder and then convolute this with an unknown function H(q) which represents the shape of the cylinder wall or one can use the FT of a basic hollow cylinder and then add the Bessel function describing these modulations on the basis of intelligent guesses. This has clear analytical advantages. The FT of a smooth walled hollow cylinder is given by [15]:

$$F(q) = R_{outer}\frac{J_1(qR_{outer})}{q} - R_{inner}\frac{J_1(qR_{inner})}{q} \quad [1]$$

The walls of this cylinder will be modulated by electron density grooves between neighbouring protofilaments, both on the inner and outer wall. Due to the 13 fold symmetry these can be expressed as J_{13} Bessel functions with arguments $J_{13}(qR_{inner}+\Delta_{inner})$ and $J_{13}(qR_{outer}-\Delta_{outer})$. The magnitudes of the Δ_{inner} and Δ_{outer} reflect the depth of the grooves on the cylinder wall. It can be calculated that the contribution due to the modulation of the inner wall falls outside the

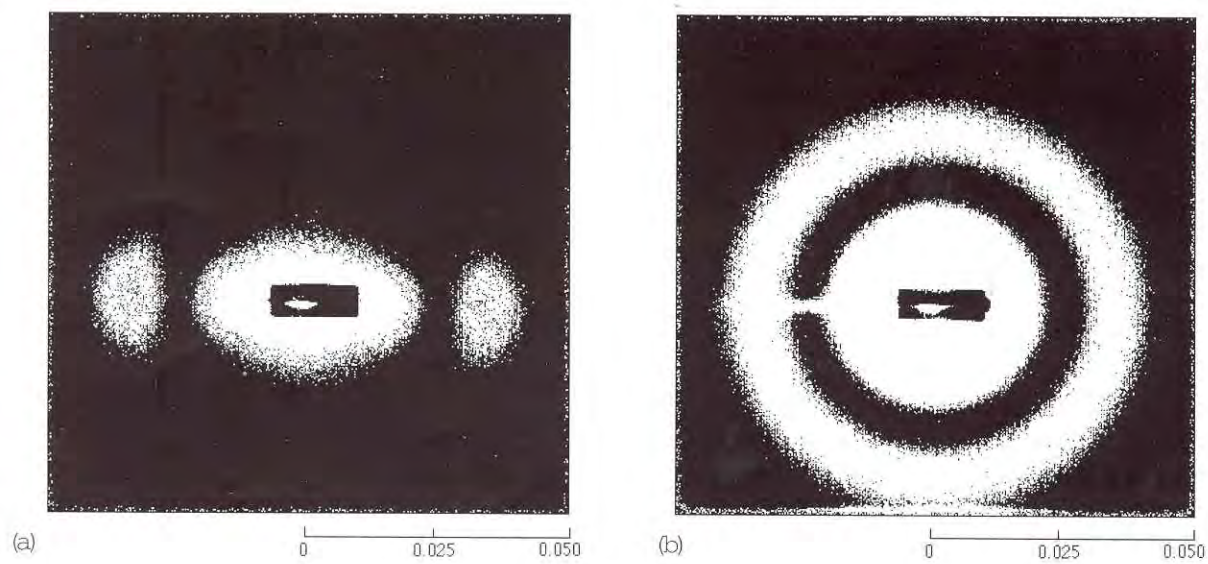

Figure 2: Small angle scattering patterns from microtubules aligned with the long axis at right angles to the X-ray beam (panel a) and with the long axis parallel with the X-ray beam (panel b). The scale is in $q=2\pi/d$ (Å^{-1}).

scattering range observed in this study, but that the modulation due to the outer wall can add scattered intensity in the observed scattering range at $q > 0.1$ Å^{-1}. An initial fit to the experimental data with an expression based on equation (1) was limited to the range $q < 0.1$ Å^{-1} and gave R_{outer}= 146±5 Å and R_{inner}= 86±5 Å. The subsequent addition of the contribution of a J_{13} Bessel function relating to the outside wall over a data range that covers the region $q > 0.1$ Å^{-1} shows that the grooves between the protofilaments are 21±3 Å deep. The results of this fitting procedure are shown in figure 3.

The first layer line can be found on a line with a meridional q-value of ≈ 0.157 Å^{-1}. As mentioned in the introduction, the degree of alignment is not extremely high and this means that in the equatorial q-range above 0.157 Å^{-1} it is possible that reflections will start to overlap. However, by using the method of first determining the accurate intensities at lower q on the equator and then fitting these with the appropriate analytical functions, it is possible to deconvolute the intensities coming from layer lines. In fact it might be better, once the equatorial diffraction pattern is accurately determined, to revert back to scattering from randomly oriented samples for the deconvolution procedure. This method is being investigated at the moment.

Figure 4 shows the low angle scattering pattern from three different tubulin concentrations obtained from samples in which the long microtubule axis was coincident with the X-ray beam. The insert shows the very low angle data, where the effects of interparticle scattering are visible. For this concentration range the (theoretical) interparticle distance has been calculated to be varying from 1800 - 2600 Å which means that it is in the dilute regime according to the definitions of [16]. To gain a better insight into these interparticle effects, simulations were performed by considering the sample to be a two-dimensional disordered fluid, which in this case is allowed due to the molecular axis being aligned. The microtubules were represented as hard, hollow discs with an inner radius of 86 Å and outer radius of 146 Å. These discs were randomly placed in a square box of side 10,000 Å. The packing of N discs into the box was carried out under the constraint that the distance between the centres of any two discs n and m in the box was $r_{nm} \geq 286$ Å, in order to avoid unphysical overlap. The initial configuration of the discs in the box was changed by forcing each disc to undergo random displacements with maximum amplitude of 16 Å. The displacement was accepted when no overlap with other discs occurred and a new configuration

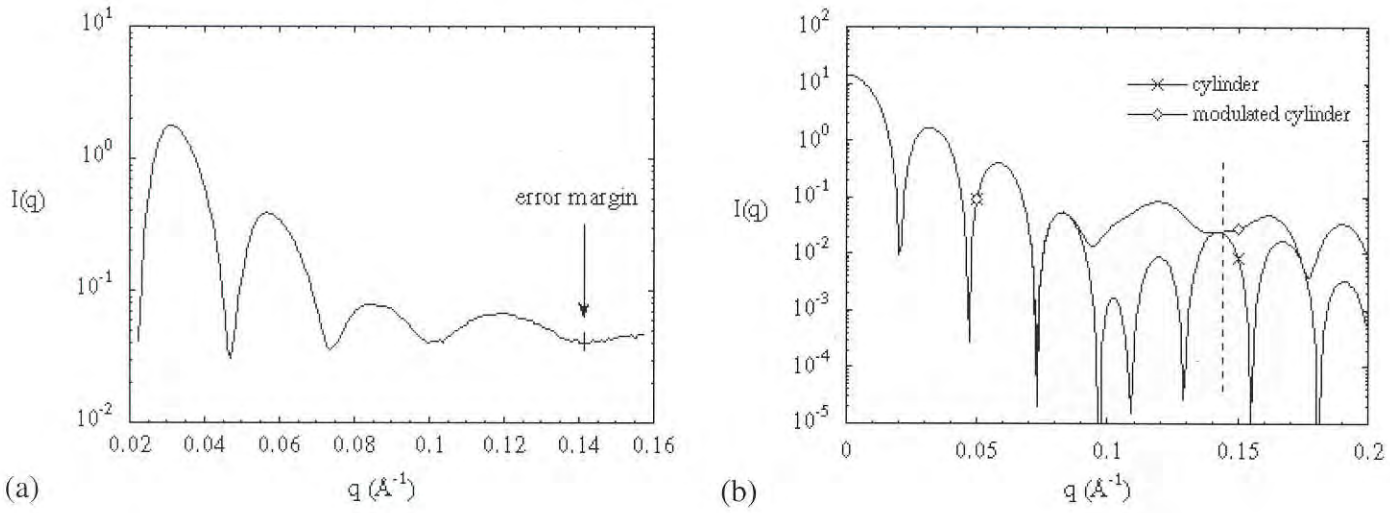

Figure 3: Scattered intensity from microtubules aligned with their long axes parallel to the X-ray beam (panel a). This is equivalent to the equatorial data obtained from a fibre diffraction pattern, but one is certain that neither systematic errors due to mathematical procedures used for correction of the angular spread of the molecules are seen nor intensity due to overlap from diffraction arcs of the layer lines. Panel b shows the best fits ($\chi^2 = 0.05$) to the data using the fitting procedure described in the text. The dotted line indicates the maximum extent of the experimental data at present. The line indicated with 'cylinder' is the contribution of two J_1 functions describing the basic cylinder. The 'modulated' curve is the real fit taking into account the modulations on the cylinder surface.

was produced. Up to 16 000 configurations were used and the diffracted intensity I_L was determined using the positions of the centres of the discs for every fifth configuration. $I_L$was calculated using the expression

$$I_L(\vec{q}) = I_D(\vec{q}) \sum_{n,m} exp[-i\vec{q}.\vec{r}]$$

where I_D is the scattered intensity from single hollow discs and q is the wave vector. We evaluated the scattered intensities from configurations containing between 50 and 700 discs, covering an average nearest centre-to-centre distance between 1000 Å and 330 Å. The number of configurations used was chosen judiciously so as to yield statistical fluctuations of less than 3% in the diffracted intensity. The differences in the simulated intensities between different concentrations are approximately a factor of 5 less than the experimental values shown in the insert of Figure 4. This can indicate that the average distance distribution is deviating from that of a completely random distribution and that actually bundles of microtubule polymers are formed. In such a scenario the interparticle scatter will be dominated by the distance distribution inside such a bundle, apparently giving a much stronger concentration effect.

Conclusions

Helical diffraction theory in combination with experiments on suitably oriented molecules allows us to introduce a step wise fitting procedure with which we first can use knowledge of the basic cylindrical structure of the molecule, then add the Bessel function terms relating to the modulations on the cylindrical surface. Thus we can overcome some problems due to the relatively poor orientation of the molecules [16].

Modelling studies describing the interparticle interference effects are being carried out at the moment. They show qualitative agreement with the experimental data, but give a strong indication that the microtubules are not randomly positioned in the samples but are forming larger bundles.

Liz Towns-Andrews and Sue Slawson of CCLRC Daresbury Laboratory have been very helpful with the fibre diffraction experiments. Joan Bordas is thanked for a useful discussion on the cylindrical nature of the microtubules.

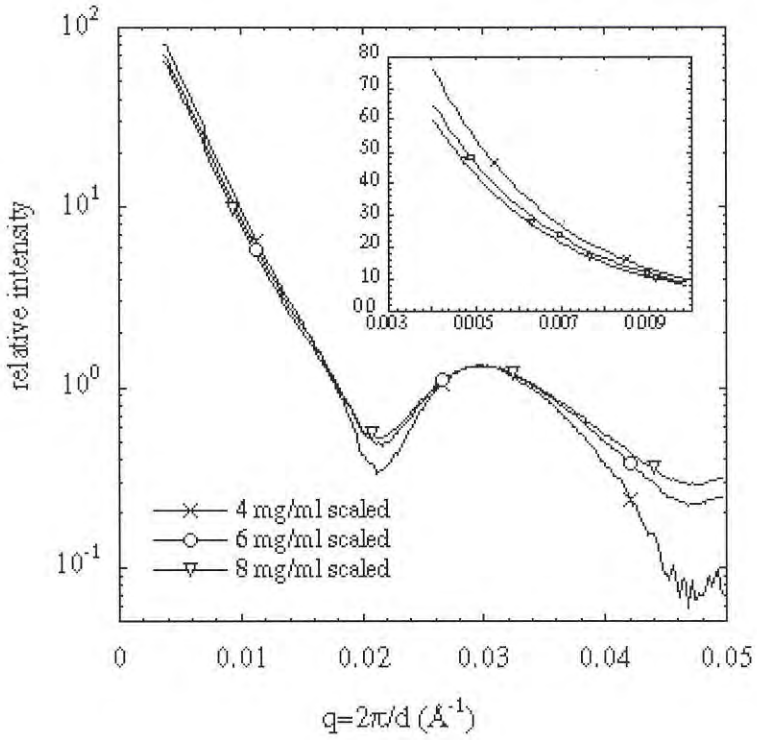

Figure 4: The low angle scattering pattern from microtubules aligned with their long axes parallel to the incident beam for 3 different concentrations. The insert is a magnification of the lowest q-range (with a linear abscissa) showing the effects of interparticle scattering. This effect is much stronger than found in simulated data. This possibly can be due to a non-random distribution of polymers in the samples through clustering in bundles. This will give rise to a locally higher concentration.

References

[1] *Structure of microtubules* (Eds K.Roberts and J.S Hyams) (Academic Press).

[2] Gittes, F., Mickey, B., Nettleton, J. and Howard, J., *J. of Cell Biol.* (1993) **120(4)**, 923-934.

[3] Venier, P., Maggs, A.C., Carlier, M.F. and Pantaloni, D., *J. Biol. Chem.* (1994) **269(18)**, 13353-13360.

[4] Pirollet, F., Job, D., Margolis, R. and Garel, J., *EMBO journal* (1987) **6(11)**, 3247-3252.

[5] Mandelkow, E., *Methods in Enzymology* (1986) **134**, 149-168.

[6] Suzuki, A., Maeda, T. and Ito, T., *Biophys. J.* (1991) **59**, 25-30.

[7] Flory, P.J., *Proc. Royal. Soc. London* (1956) **A234**, 73-89.

[8] Bras, W., Diakun, G.P., Díaz, J.F., Maret, G., Kramer, H., Bordas, J. and Medrano, F.J., *Biophysical Journal* (1998) **74(3)**, 1509-1521.

[9] http://www.dl.ac.uk/SRS/CCP13

[10] Denny, R.C., CCLRC Daresbury laboratory private communication.

[11]Klug, A., Crick, F. and Wyckoff, H., *Acta. Cryst.* (1958) **11**, 199-213.

[12] Amos, L.A. and Klug, A., *J. Cell. Sci.* (1974) **14**, 523-549.

[13] Andreu, J.M., Bordas, J., Díaz, J.F., Garcia de Ancos, J., Gil, R., Medrano, F.J., Nogales, E., Pantos, E. and Towns-Andrews, E., *J. Mol. Biol.* (1992) **226**, 169-184.

[14] Glatter, O., in *Small Angle X-ray scattering* (Eds Glatter, O. and Kratky, O.) (Academic Press, 1982).

[15] Vainshtein, B.K., in *Diffraction of X-rays by chain molecules* (Elsevier, 1966).

[16] Edwards, S.F., *Proc. Phys. Soc.* (1966) **88**, 265-281.

* A part of the problem due to the poor orientation might be overcome by keeping the samples during the experiments in a magnetic field. Preparations, in collaboration with the High Magnetic Field Laboratory (Grenoble), to use a 10 T split coil magnet are in an advanced state. Interested people can contact W. Bras.

The ups and downs of native cellulose structure

R.P. Millane

Whistler Center for Carbohydrate Research and Computational Science and Engineering Program, Purdue University, West Lafayette, Indiana 47907-1160, U.S.A.

Cellulose was one of the first materials to be studied by X-ray fibre diffraction. Although structural studies have continued over the last 60 years, ambiguities have persisted with regard to chain packing and multiple phases of native cellulose, and only recently have these been resolved. X-ray fibre diffraction has played a dominant role, although other techniques have also provided essential information.

Cellulose is the major constituent of most land plants, is the most abundant natural compound, and is an important commercial raw material. It is a linear polymer of 1→4-linked β-D-glucose with a degree of polymerisation >3000. In native cellulose, the molecules are aligned to form fibres, some regions of which have an ordered crystalline structure. The crystalline regions vary in size, are mechanically strong, and are resistant to chemical and enzymatic attack. Cellulose is a structural component in plant and other systems and is used widely in industry. Artificial cellulose derivatives are also used extensively in a variety of industries. Although plant sources are the most familiar, cellulose is also present in bacteria, fungi and algae. Due to its ubiquity and importance, and its polycrystalline nature, cellulose was one of the first materials to be studied by X-ray fibre diffraction analysis. The first such studies were reported by Meyer and Misch [1] in 1937, on plant cellulose from ramie. They determined that the unit cell is monoclinic, that two molecules pass through the unit cell, and suggested that the chains have two-fold screw symmetry. Further studies, including data from electron diffraction and infrared spectroscopy, and also from algal celluloses, supported the results of Meyer and Misch, but with some differences [2-4]. Most notably, diffraction patterns from the algal celluloses contained a few, extra, weak reflections. These were attributed to the *a* and *b* unit cell dimensions being twice those of the plant celluloses. This "large" unit cell therefore contains eight molecules, and there were presumably small differences between the packing and/or molecular

conformations of the chains that produce small deviations from the symmetry of the small two-chain unit cell. Interestingly (this will be discussed later), Sarko and Muggli [3], in 1974, noted that the equatorial reflections (that include some of the "extra" large unit cell reflections) on an electron diffraction pattern from a bacterial cellulose could all be indexed on the basis of a one-chain triclinic unit cell.

The above discussion refers to "native" cellulose, which occurs only as a result of biosynthesis, and is referred to as cellulose I. Although this article is concerned only with native cellulose, we note, for completeness, that various treatments of cellulose produce a variety of polymorphic crystal structures [5]. These all retain the same molecular structure of native cellulose, but differ in the crystal packing and the intermolecular hydrogen bonding pattern. The different allomorphs are referred to as cellulose II, III, and IV. Cellulose II is produced by mercerization (swelling in alkali) or regeneration (precipitation) of cellulose I, and has a two-chain monoclinic unit cell, but of different cell dimensions to those of cellulose I. The cellulose I $\rightarrow$ II transition can be conducted in the solid state, is irreversible, and corresponds to a parallel to antiparallel transition in the packing. There are two forms of cellulose III that are obtained by treating cellulose I or II with liquid ammonia, and the molecules pack in two different two-chain monoclinic unit cells of (again) different dimensions. Two forms of cellulose IV are obtained by heating cellulose I or II with gylcerol, and the molecules pack in two different two-chain orthorhombic unit cells.

Returning to cellulose I, two chains pass through the monoclinic unit cell at the points (0,0) and (1/2,1/2) in the *a*-*b*-plane, and the space group is P1. Within these constraints, there are three possible packing arrangements of the two chains. First, the chains may be "parallel" or "antiparallel," as a result of the directionality of the cellulose molecule. Second, because of the monoclinic angle, there are two different parallel packings, that are referred to as "parallel up" and "parallel down". That there are two distinct parallel packings appears to have been first recognised by Gardner and Blackwell [4]. Because the monoclinic angle $\gamma = 97°$ is close to 90°, the differences between the up and down packings are small, but are stereochemically significant.

The first quantitative (i.e. based on an objective numerical refinement of crystal structure models against X-ray and steric data) X-ray structures of cellulose I were by Sarko and Muggli [3] and Gardner and Blackwell [4], both in 1974, for *Valonia* cellulose. These are referred to here as the SM and GB *Valonia* structures, respectively. In both of these studies, the weak "large cell" reflections were excluded from the analyses and the structure determined on the basis of the small one-chain unit cell. Following these studies, in 1980 Woodcock and Sarko [6] determined the structure of native ramie cellulose (referred to here as the WS ramie structure). These three structures emerged as the definitive crystal structures of native cellulose. They consistently defined a ribbon-like 2_1 structure for the cellulose molecule, two of which packed parallel in the unit cell, and the formation of hydrogen-bonded sheets. However, they were inconsistent regarding the packing (up or down) of the sheets, which are stabilised by van der Waals forces. Unfortunately, this was not generally realised at the time since the differences (1) are rather small, and (2) were confused by the use of differing conventions for describing the packings in the different studies. The confusion was due to the SM and GB *Valonia* structures both being described as parallel up, whereas, in fact, they actually correspond to opposite packing polarities. Although the same definitions of "up" packing of the chains relative to the *c*-axis was used, the unit cell constants were defined such that $a < b$ for the SM *Valonia* structure, whereas the GB structure was defined with $a > b$. This effected a reversal in the polarities between the two structures. In what has now become the standard convention ($a < b$), the SM structure is parallel up, whereas the GB structure is parallel down. This inconsistency went largely unnoticed until it was pointed out by French in 1989 [7]. Furthermore, Sarko and Muggli did not, in fact, consider the parallel down packing in their analysis. The WS ramie cellulose I structure is packed parallel up. There was also, therefore, a question as to whether the plant and algal celluloses have the same, or different, packings. Consequently, even in the 1990s, no definitive X-ray structure of *Valonia* cellulose I actually existed. Furthermore, since *Valonia* gives the best X-ray data, the precise packings of all the native celluloses were in doubt.

There was some discussion in the late 1980s that inconsistencies in the X-ray structures of cellulose I might be due to the paucity of the X-ray data, difficulties in accurately measuring the X-ray data, and differences between the different refinement

protocols used. However, Millane and Narasaiah showed, at least for ramie, that the WS structure was well-supported even if one considered other X-ray data sets [8], or used different refinement programs [9].

In the late 1990s, information on the up versus down packing of native cellulose began to emerge from results obtained using other techniques. Molecular mechanics and dynamics calculations showed a preference for the parallel up structure [10-12]. An intricate experiment by Koyama *et al.* in 1997 involving electron diffraction, cellobiohydralase digestion, and silver staining of an algal cellulose gave very good direct evidence for parallel up packing [13]. The lingering inconsistent X-ray results remained however.

The question of up versus down packing, and reconciliation of the X-ray results, was finally settled by Finkenstadt and Millane in 1998 by conducting a careful reanalysis of the SM and GB X-ray data [14]. Sterically flexible models of each possible packing were subjected to least-squares joint refinement against the two X-ray data sets and steric restraints. Analysis of both the X-ray agreement and the steric compression of the refined models showed that both data sets unequivocally support parallel up, and not parallel down, structures. The details can be found in Reference 14. A successful analysis of the structure is possible now (as opposed to in 1974) because refinement methods (and larger computers) available today can accommodate better joint steric/X-ray refinement of more complete and flexible molecular and crystal structure models.

The parallel up packing of native cellulose appears, therefore, to be ubiquitous throughout the plant, algal and bacterial celluloses. Views of the refined cellulose I crystal structure are shown in Fig. 1. An illuminating way of looking at the differences between up and down packing is to consider only up polarity of the chains relative to the *c*-axis, and then the down packing is obtained by changing the monoclinic angle (γ) of the unit cell from 97° to 83° [14]. To investigate the basis of the preference for parallel up over parallel down packing, cellulose chains were packed together as closely as possible without allowing steric anomalies, for different fixed values of γ [14]. The packing densities of the resulting structures were calculated as a function of γ, and the results are shown in Fig. 2. It is clear from the figure that the parallel up packing (γ = 97°) is

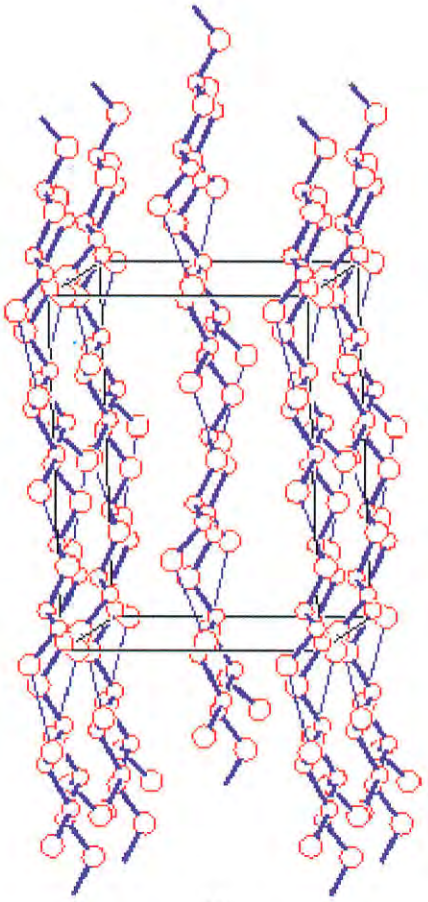

(a)

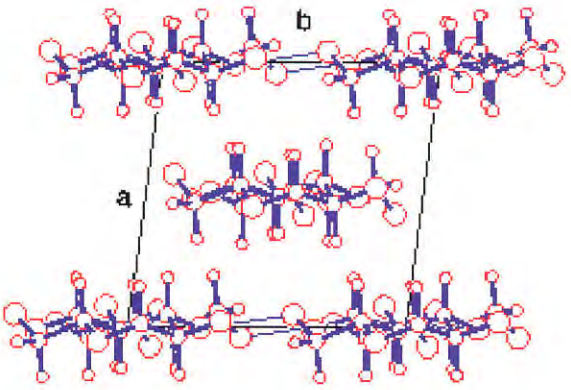

(b)

Figure 1: Views of the refined cellulose I crystal structure **(a)** obliquely to, and **(b)** along, the *c*-axis [14]. Thin lines show hydrogen bonds. The hydrogen atoms are excluded from (a) for clarity.

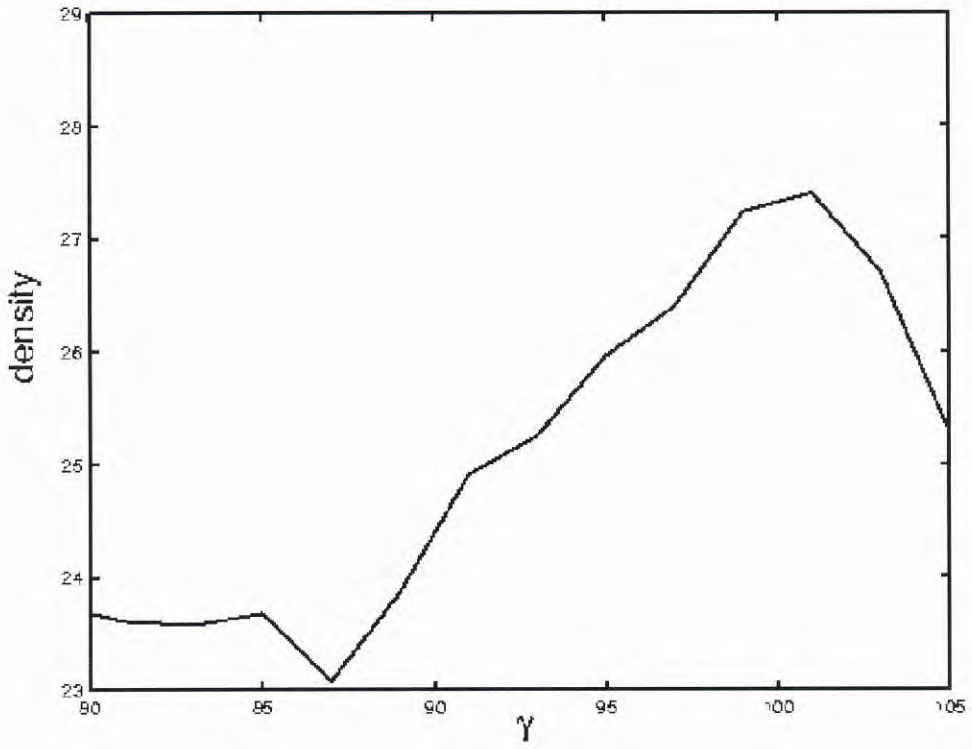

Figure 2: Packing density (arbitrary units) for sheets of cellulose molecules packed in a crystalline array as a function of the monoclinic angle γ [14].

close to the maximum packing density, whereas the parallel down packing ($\gamma = 83°$) is well away from the maximum. Of course the density so calculated is only approximate, but the trend is clear.

Is the structure of native cellulose now completely understood? Unfortunately no! In 1991, Sugiyama *et al.* [15] showed, using electron diffraction, that most celluloses are actually a mixture of two crystalline allomorphs. One of these is referred to as cellulose Ib and corresponds to that which packs in the two-chain monoclinic unit cell as described above. The other allomorph, referred to as cellulose Ia, packs in a one-chain triclinic unit cell. The two unit cells are intimately related as shown in Fig. 3, and lead to an axial shift of $c/2$ in every second sheet of cellulose molecules, between the two allomorphs. This results in a subtle difference in the packings of the two allomorphs. Algal celluloses are rich in the Ia allomorph and plant celluloses are rich in Ib. The triclinic unit cell explains the extra reflections observed in diffraction patterns from algal celluloses, that were originally attributed to a much larger monoclinic unit cell. The bimorphic structure also explains nmr data first reported in 1984 [16] that indicated the presence of two phases. The crystal structure of cellulose Ia has not been determined, but the definitive Ib structure and the relationship between the two unit cells fixes the structure in all but the fine details. There are still many questions concerning native cellulose however, including the distribution of the two allomorphs in nature, the biosynthetic mechanisms leading to the two allomorphs, and the biological function of the two subtly different packings. Finally, it is worth mentioning that Sarko and Muggli's triclinic unit cell [3], although different to that now derived from electron diffraction, did incorporate the successive $c/4$ shift of adjacent cellulose sheets more recently determined for the triclinic structure. This insightful observation 25 years ago appears to be overlooked in the modern literature.

X-ray fibre diffraction analysis of cellulose structure has a long history – spanning 60 years and continuing. From a primary structure point of view, cellulose is a simple molecule. However, it is semicrystalline and adopts a large number of

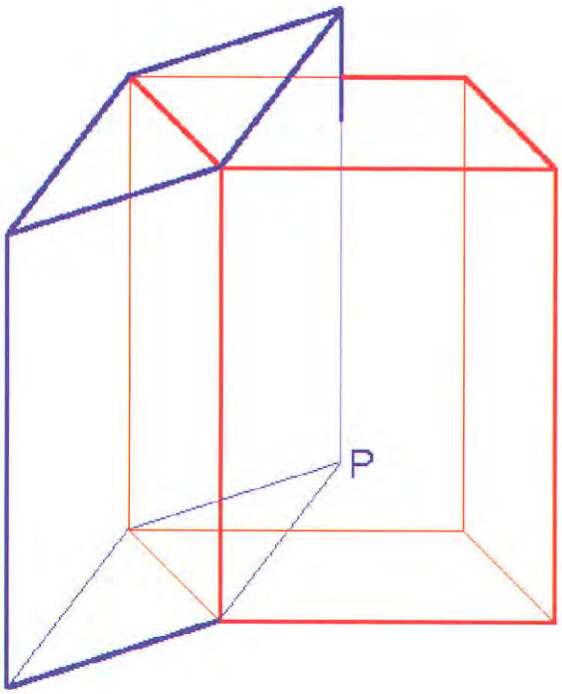

Figure 3: Relationship between the monoclinic unit cell (red) for cellulose Ib, and the triclinic unit cell (blue) for cellulose Ia. The point P has fractional coordinates (1/2,1/2,1/4) in the monoclinic system.

allomorphs. The small crystallite dimensions, inherent disorder, biphasic nature, and the presence of amorphous material mean the X-ray data from cellulose are low resolution and "murky." However, even under these conditions, X-ray fibre diffraction analysis has produced an enormous amount of essential structural information on this important material. Structural studies of cellulose demonstrate the truth of Arnott's assertion [17] that in the application of fibre diffraction "... with today's technology scrupulously applied, most gross errors are detectable."

References

[1] Meyer, K.H. and Misch, L., *Helv. Chim. Acta* (1937) **20**, 232-244.

[2] Nieduszynski, I. and Atkins, E.D.T., *Biochim. Biophys. Acta* (1970) **222**, 109-118.

[3] Sarko, A. and Muggli, R., *Macromolecules* (1974) **7**, 486-494.

[4] Gardner, K.H. and Blackwell, J., *Biopolymers* (1974) **13**, 1975-2001.

[5] Millane, R.P., in *Frontiers in Carbohydrate Research 2* (Ed. R. Chandrasekaran) 168-190 (Elsevier, London, 1992).

[6] Woodcock, C. and Sarko, A., *Macromolecules* (1980) **13**, 1183-1187.

[7] French, A.D. and Howley, P.S., in *Cellulose and Wood* (Ed C. Schuerch) 159-167 (Wiley, New York, 1989).

[8] Millane, R.P. and Narasaiah, T.V., in *Cellulose and Wood* (Ed C. Schuerch) 39-51 (Wiley, New York, 1989).

[9] Millane, R.P. and Narasaiah, T.V., *Polymer* (1989) **30**, 1763-1767.

[10] Aabloo, A., French, A.D., Mikelsaar, R.H. and Pertsin, A.J., *Cellulose* (1994) **1**, 161-168.

[11]Heiner, A.P., Sugiyama, J. and Teleman, O., *Carbohydr. Res.* (1995) **275**, 207-223.

[12] Kroon-Batenburg, L.M.J., Bouma, B. and Kroon, J., *Macromolecules* (1996) **29**, 5695-5699.

[13] Koyama, M., Helbert, W., Imai, T., Sugiyama, J. and Henrissat, B., *Proc. Natl. Acad. Sci. USA* (1997) **94**, 9091-9095.

[14] Finkenstadt, V.F. and Millane, R.P., *Macromolecules* (1998) **31**, 7776-7783.

[15] Sugiyama, J., Vuong, R. and Chanzy, H., *Macromolecules* **24** (1991) 4168-4175.

[16] Atalla, R.H. and van der Hart, D.L., *Science* (1984) **223**, 283-285.

[17] Arnott, S., in *Biopolimeri* (Associazione Italiana di Scienza e Tecnologia delle Macromolecole) Chapt. 23 (Italy, 1984).

CCP13 Software Development

M.W. Shotton[1,2], R.C. Denny[1] and V.T. Forsyth[3]

1 CLRC Daresbury Laboratory, Daresbury, Warrington, Cheshire WA4 4AD, U.K.

2 Biophysics Section, Blackett Laboratory, Imperial College, London, U.K.

3 Institut Laue-Langevin, BP 156 F-38042, Grenoble Cedex 9, France.

There have been significant changes to two of the programs in the CCP13 suite. The CONV program has been replaced by XCONV, which is driven by an OSF/Motif-based graphical user interface (GUI). XCONV provides for the conversion of various image data files to BSL format and is aimed at being more user-friendly than CONV, especially in the case of multiple file processing. There have also been several changes to XFIX, including the

incorporation of background estimation techniques. All programs in the CCP13 suite have now been developed for use on LINUX operating systems in addition to SOLARIS, IRIX and OSF. All CCP13 software can be downloaded from the web pages at http://www.dl.ac.uk/SRS/CCP13.

1 Introduction

1.1 XCONV

XCONV can be used to gain access to other programs in the CCP13 suite, such as XFIX, by providing for the conversion of image data files to BSL format. BSL format is the common input/output format for two-dimensional diffraction data used by CCP13 programs. The BSL file format is described in the BSL manual at http://www.dl.ac.uk /SRS/NCD/manual.bsl.html. XCONV replaces the CONV program, and has been made more user-friendly by the addition of an OSF/Motif-based GUI (see Figure 1) and by the incorporation of some additional features that were not available in CONV, including multiple file operations and user-defined data conversion profiles that can be saved and reused.

1.2 XFIX

XFIX has been designed for the preliminary processing of two-dimensional fibre diffraction data. Information such as the pattern centre, detector and fibre orientation can be estimated and refined, lattice points can be superimposed on the pattern and integrated slices or scans through the pattern can be plotted and fitted. It is now also possible to use XFIX to estimate the background component of the diffraction pattern by one of the following three techniques:

(i) Paul Langan's "roving window" method.
(ii) Calculation of a circularly symmetric background.
(iii) Calculation of a "smoothed" background through iterative low-pass filtering, based on the method of M.I. Ivanova and L. Makowski [1].

Methods (i) and (ii) were previously available within the LSQINT data-fitting program, while method (iii) is new to the CCP13 suite.

2 Data processing

2.1 Data conversion to BSL format using XCONV

The XCONV GUI is shown in Figure 1. It is split into two sections relating to the input image data file(s) and the output BSL file. The operation of the GUI is described in detail in the help pages that may be downloaded with the executable from the CCP13 web site at http://www.dl.ac.uk/SRS/CCP13 or, alternatively, can be viewed at http://www.dl.ac.uk/SRS/CCP13/program/xconv.html. The main improvements over the command line-driven program CONV are discussed below.

2.1.1 Multiple input files

Data file(s) may be selected for input to XCONV by entering the path and filename directly in the text window provided or by using the File Selection Tool, which is opened by clicking on the "Browse" button. In order to convert a series of similar data files (i.e. collected on the same detector), whose filenames differ only in their run numbers, the wildcard characters "%" and "#" may be inserted in the filename. "%" marks the position in the filename where the run number is to be inserted. If the run number is to be written into a fixed number of positions in the filename, "#" is used to indicate the position of a digit.

For example, my_data_%.dat would expand to:
my_data_1.dat, my_data_2.dat, ... , my_data_10.dat

whereas my_data_###.dat would expand to:
my_data_001.dat, my_data_002.dat, ... , my_data_010.dat

The first and last run numbers and increment can be entered in the fields provided. The multiple input files are converted and written to consecutive frames of the output BSL data file.

2.1.2 Data types

The following input data types can be selected from the pull-down menu:

(i)	float	float (4 bytes)
(ii)	int	unsigned int (4 bytes)
(iii)	short	unsigned short int (2 bytes)
(iv)	char	unsigned char (1 byte)

(v) smar small MAR image plate (1200×1200 pixels)
(vi) bmar large MAR image plate (2000×2000 pixels)
(vii) fuji Fuji image plate
(viii) rax2 R-Axis II image plate
(ix) psci Photonics Science CCD

If the input file type corresponds to one of the primitive types (i) to (iv) above, then the user must also input the dimensions of the input data, the number of bytes to skip (e.g. header information) and the pixel aspect ratio. These are entered automatically in the case of data types (v) to (ix).

2.1.3 Saving user-defined data conversion profiles

The "Save profile" button may be used to save the contents of the following fields to an ascii file:

(i) File type
(ii) Input pixels and rasters
(iii) Bytes to skip
(iv) Pixel aspect ratio
(v) Dynamic range for Fuji image plates
(vi) Byte swapping on/off
(vii) Output pixels and rasters

This saved profile can then be reused at a later stage with the "Load profile" button.

2.2 Background subtraction using XFIX

There are three methods for estimating the background component of a diffraction pattern using XFIX:

(a) Paul Langan's "roving window" method.
(b) Calculation of a circularly symmetric background.
(c) Calculation of a "smoothed" background through iterative low-pass filtering, based on the method of M.I. Ivanova and L. Makowski [1].

These can be selected from the "process" menu by clicking on "background". All three methods require

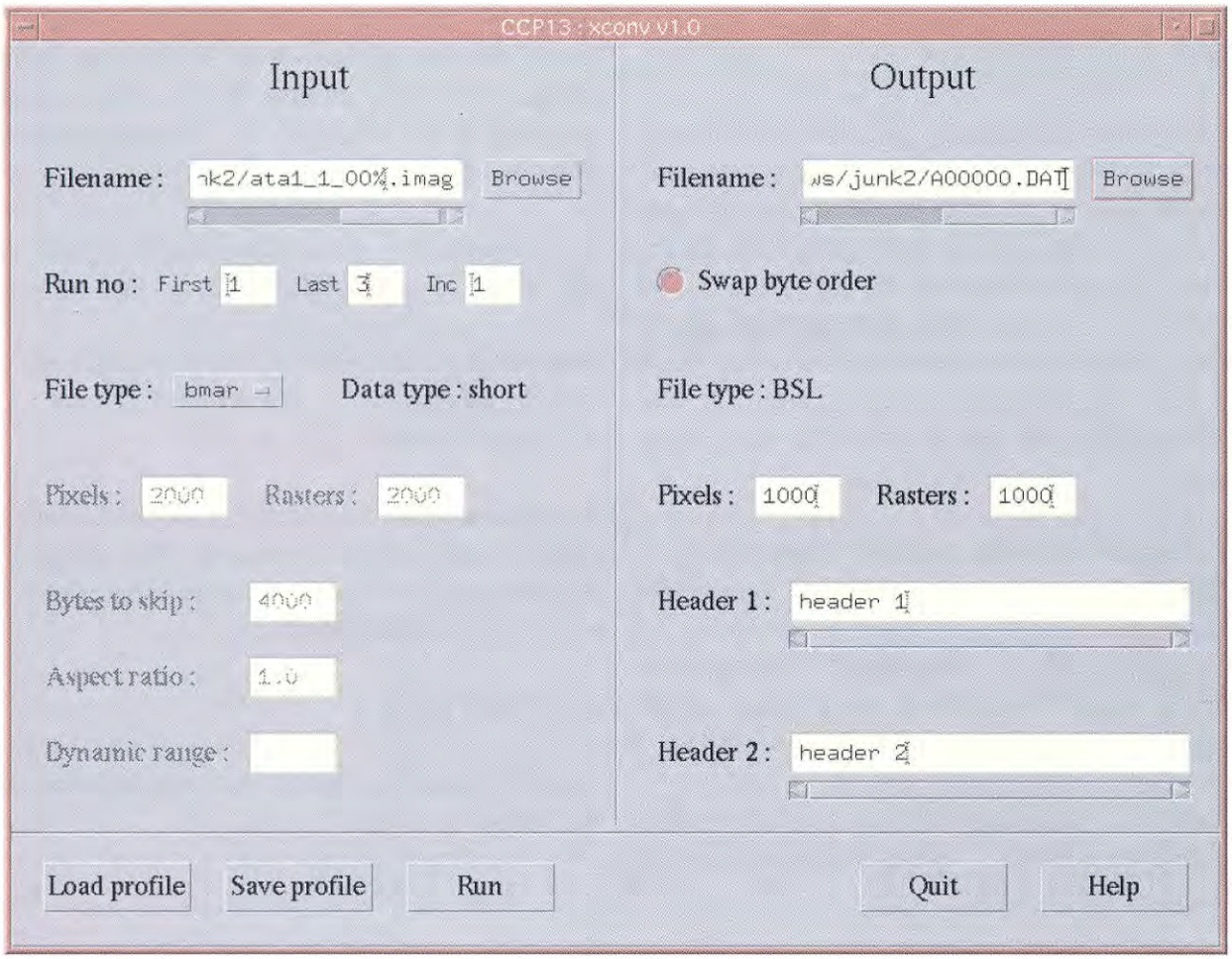

Figure 1: The XCONV GUI

the user to input the pattern centre and the extent of the pattern (minimum and maximum radii in pixel units) in relation to the centre. Pixel values outside these limits will be ignored in the background estimation. If the diffraction pattern is not circular and centred around a single point, then it is possible to discard values less than a user-input minimum so that, for example, all values less than or equal to 0.0 are ignored in the background calculation. By using the BSL program from the NCD software suite, it is possible to mask the areas of the image that are not of interest (for example by assigning a large negative value to unwanted pixels) and discarding these values in the background calculation.

The details of the different background estimation techniques are discussed below. In each case, once processing is completed, the user is prompted to view the calculated background. This will open a new XFIX interface with a 2-frame BSL file loaded. The first frame in this file is the estimated background and the next frame is the diffraction data with the estimated background subtracted. This provides a visual indication of the "goodness of fit" of the calculated background. The calculated background in frame 1 of the file can then be processed further using any of the three background estimation techniques. In this way, different background subtraction methods can be used consecutively if desired. Finally, the data minus background frame can be used with a fitting program such as LSQINT in order to measure the reflection intensities.

It should be noted that these methods of background estimation can be very time-consuming when used with a large image (e.g. 2000×2000 pixels). It may often be worthwhile to scale down the dimensions of the diffraction pattern using XCONV (e.g. to 200×200 pixels) to find the optimum parameters to be used in the process before operating on the full-size image.

2.2.1 Roving window method

The roving window background subtraction method of Paul Langan estimates the background by moving a window (of size input by the user) across the collected data. The pixel values within this window are sorted by value and those in the user-selected range are taken as background (except pixel values lying outside the pattern extents or specified by the user as values to discard). The average pixel value within this range is then assigned to be the estimated background at the centre of the window. Finally, a smoothing spline under tension is fitted to fill in the gaps between window centres.

2.2.2 Circularly-symmetric background

A circularly-symmetric background can be formed by the radial binning of pixel values followed by averaging those pixel values lying within a specified range. This average value is assigned to the particular radius and a smoothing spline under tension is fitted to yield the estimated background

2.2.3 Smoothed background - Iterative low-pass filtering

This method of background subtraction is based on that of M.I. Ivanova and L. Makowski [1]. It takes advantage of the fact that the background of a fibre diffraction pattern is typically composed of lower spatial frequencies than the diffraction maxima. Hence an iterative low-pass filter can be applied to separate the two components on the basis of their frequencies. The estimated background depends on the frequency limit of the filter in both X and Y.

The application of the low pass filter is achieved by the convolution of the observed diffraction pattern with a box car or gaussian function (the smoothing function) having an average value of unity taken over the number of pixels it occupies and a value of zero elsewhere. This function is convoluted with the real data at each pixel within the pattern limits (excluding pixels that are specified by the user as to be discarded). The result of applying this filter is an overestimated background, containing some intensity from the diffracted maxima (e.g. Figure 2(b)). This overestimated background is then subtracted from the real data to leave the diffraction maxima whose intensities are now underestimated (e.g. Figure 2(c)). Positive pixel values in the image resulting from this subtraction are then subtracted from the original data to yield the next estimate of the background. This is then convoluted with the smoothing function and the procedure is repeated, with images of the original data minus estimated background providing a visual indication of the "goodness of fit" of the estimated background. The results of applying the iterative low-pass filter to high-angle fibre diffraction data collected from the D conformation of DNA are shown in Figure 2.

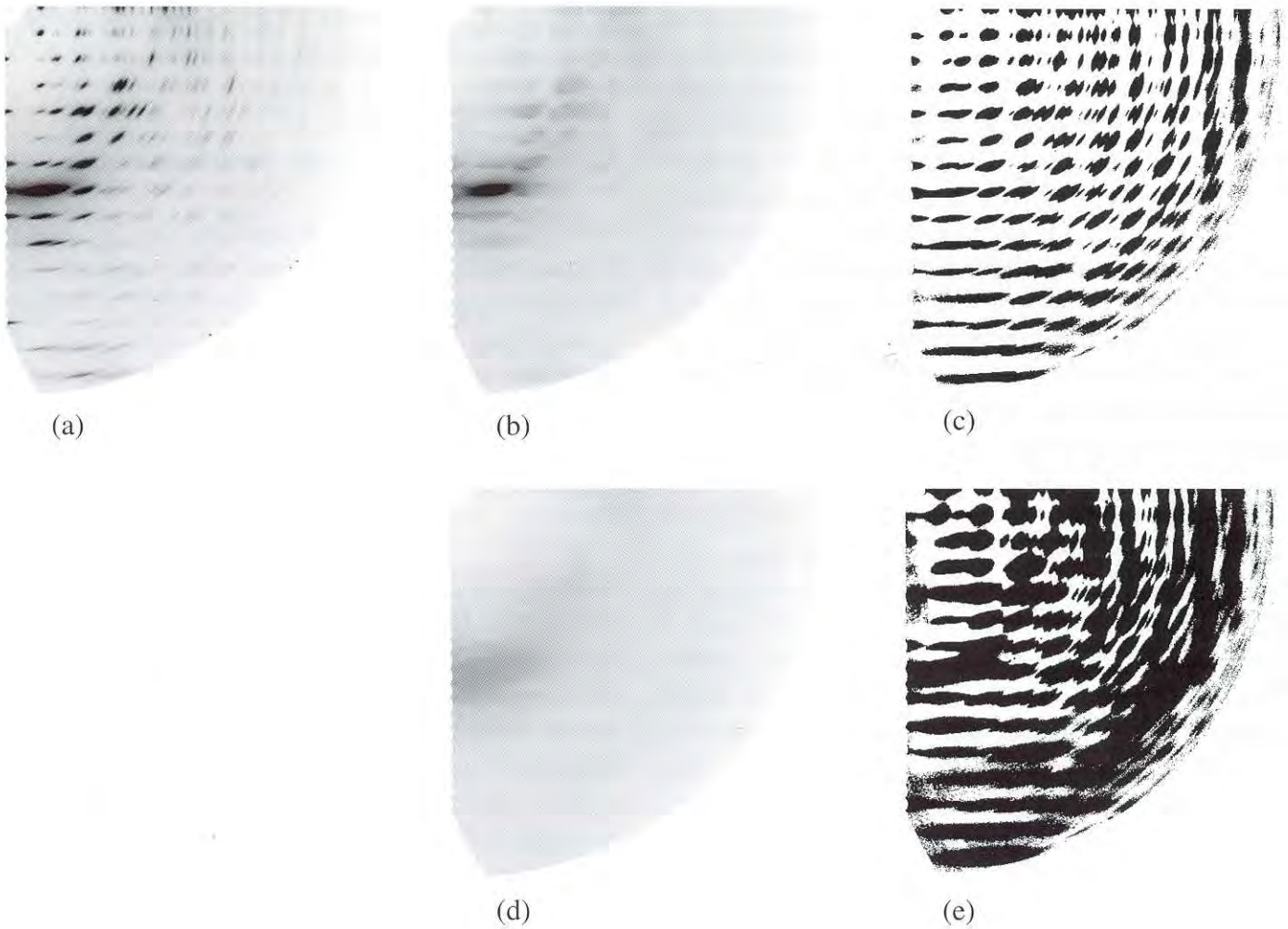

Figure 2: **(a)** High-angle fibre diffraction data collected from the D conformation of DNA (displayed at threshold levels of 2000, 0). **(b)** The estimated background following one cycle of low-pass filtering (display thresholds 2000, 0). **(c)** is the pattern (a) minus the estimated background (b) (display thresholds 1, 0). **(d)** The estimated background following five cycles of iterative low-pass filtering (display thresholds 2000, 0). **(e)** shows pattern (a) minus estimated background (d) (display thresholds 1, 0).

There are problems that exist with this method of background estimation at the edge of the pattern where information cannot be obtained for the convolution. This can lead to edge effects (typically an underestimation of the background), which become more pronounced with each cycle of filtering. In this case, it is possible to import a background calculated by another method to be used as the final background estimate at the edges of the pattern. This is then left as constant throughout each cycle of filtering. The backgrounds calculated by the different methods are then merged by fitting a smoothing spline under tension.

Once the background estimation process has been completed, the user will be prompted to view the estimated background and original pattern minus estimated background as described above. This will open a new XFIX interface. Once the estimated background has been inspected, the user may then choose to perform more iterations of filtering. Hence it is possible to view the estimated background after each iteration if desired.

References

[1] M.I. Ivanova and L. Makowski, *Acta Cryst.* (1998) **A54**, 626-631.

Myosin head configurations in relaxed, active, rigor and S1-labelled fish muscle; Evidence for characteristically distinct states

J. Harford[1,4], R.C. Denny[1,3], L. Hudson[1], R. Mendelson[5], E. Morris[2] and J. Squire[1]

1 Biophysics Section, Blackett Laboratory, Imperial College, London, U.K.
2 Biochemistry Department, Imperial College, London, U.K.
3 CLRC Daresbury Laboratory, Daresbury, Warrington, Cheshire WA4 4AD, U.K.
4 Biophysics Dept., King's College, London, U.K.
5 Cardiovascular Research Institute, UCSF, San Francisco, U.S.A.

Introduction

Movement in all cells, whether they are muscle cells or not, is mediated by the action of motor proteins, such as myosin heads and kinesin, on filamentous 'tracks', respectively actin filaments (polymers of actin molecules) and microtubules (polymers of tubulin). In each case the motor protein is thought to attach to its track, to change its conformation in some way, thus producing movement, and then to detach again ready for another attachment - detachment cycle. In all cases the cycle is associated with the hydrolysis of ATP. Although a great deal has been learnt in the recent past about the atomic structures of some of these proteins [e.g. for muscle 5-7], it is still not clear exactly how movement is produced. Studies of intact muscle have the advantage that some muscles are extremely highly organised and they give rise to detailed X-ray diffraction patterns that, in principle, can be solved to yield details of the molecular organisation in the muscle. Muscle states can also be altered at will, so, for example, a muscle can be depleted of ATP, which normally promotes detachment of myosin heads from actin, so that long-lived attached states of myosin heads on actin are produced. Thus, although the microtubule motor systems can only be studied sensibly at tubule level in, for example, the electron microscope, the myosin/actin system can be studied by a variety of different structural methods which can even provide time-resolved structural details of the myosin motor in action [e.g. 1-4, 9-14].

Two particular muscle systems have been discovered that because of their superb degree of order provide technical advantages in structural studies. In the case of vertebrate muscles it is the muscles of fish that are particularly useful for this [1-4, 9-12], whereas in the case of the invertebrates it is insect flight muscles that are the most beautifully organised of all [15,16]. Figure 1(a) gives a generalised view of a muscle sarcomere, which is shown to comprise overlapping arrays of actin filaments and myosin filaments. The myosin heads (crossbridges) form projections on the myosin filament surface. In this position they can attach to, possibly 'swing' on, and then detach from neighbouring actin filaments in a typical contractile cycle. Figure 1(b) summarises the ATPase cycle associated with this mechanical crossbridge cycle. The work reported here concerns the myosin head/actin interactions in defined states of fish skeletal muscle (the fin muscles of plaice, Pleuronectes platessa) in order to provide a detailed insight into the myosin head cycle on actin in active muscle.

Relaxed Fish Muscle

The positions of the myosin heads in relaxed fish muscle have been determined by analysis of low-angle X-ray diffraction patterns (Figure 2) recorded on beamlines 16.1 and 2.1 at the CCLRC Daresbury Synchrotron Radiation Source [1-4]. Head shape was defined from the study of S1 crystals [5], with variable head configurational parameters given on each of the three different 3-fold symmetric 143Å-spaced 'crowns' of myosin heads within the 429Å axial repeat of the myosin filaments. Diffraction patterns were stripped using CCP13 fibre diffraction software [8] to give 56 independent intensity values out to a resolution of about 65Å. Searches and optimisation [3,4] were carried out using simulated annealing and local refinement procedures to give a 'best fit' structure with a crystallographic R-factor of about 4% (Figure 3(a)). The heads in this structure were all the same way up (i.e. with similar rotations around their own long axes), but they had a small range of axial tilts. The preferred structure also defined the orientation of the whole myosin filament array within the fish muscle A-band unit cell (Figure 3(b)). This positioned the myosin heads close to but not touching the adjacent actin filaments [3,4,9].

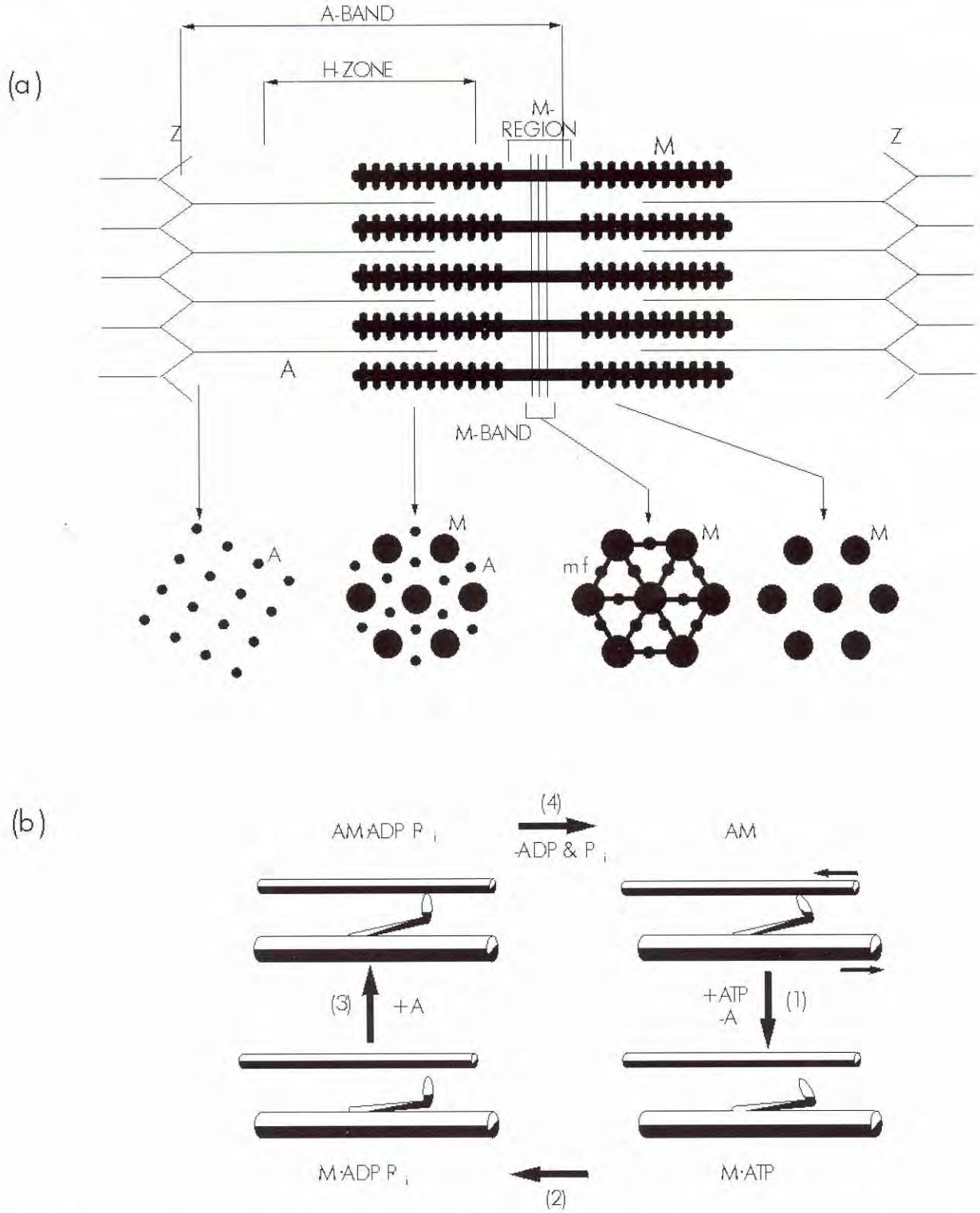

Figure 1: **(a)** Schematic diagram of a muscle sarcomere (Z to Z), showing the overlapping arrays of actin and myosin filaments. Sarcomere shortening occurs when these arrays slide past each other, powered by the action of myosin heads. **(b)** Correlation of a simplified mechanical cycle of myosin heads on actin and the corresponding stages in the hydrolysis of ATP [13].

Different Muscle States with Attached Myosin Heads

Head configurations are being determined for rigor and 'S1-decorated' rigor fish muscle (i.e. with no bound nucleotide - S1 are myosin heads proteolytically cleaved from the myosin molecule). This is being carried out by combined X-ray diffraction and electron microscopy studies of skinned muscle in rigor solution (Figure 2(c)), and in rigor solution, but also containing extrinsic myosin S1, in this case chicken papain S1 [9-11] (Figure 2(d)). Computed 3-D reconstructions (Figure 3(c)) of acto-S1 using X-ray amplitudes (Figure 2(c)) and phases from electron microscopy (courtesy R. Milligan) are informative and help to analyse the X-ray diffraction data that extend axially to about 10 Å resolution (see Harford *et al.* [11]).

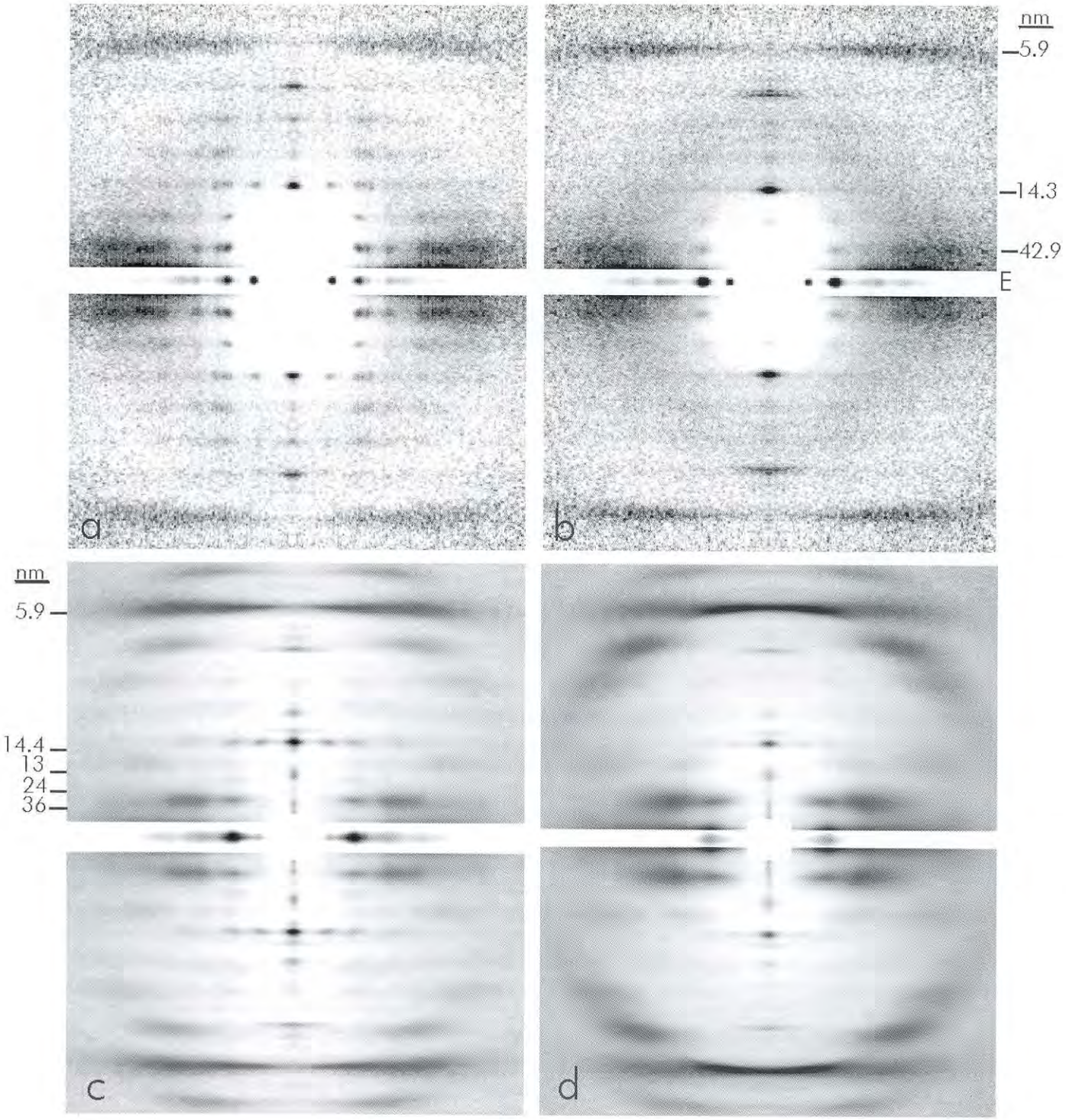

Figure 2: Low-angle X-ray diffraction patterns (fibre axis vertical) recorded from plaice fin muscles in a variety of static states. All patterns shown here were obtained at the CLRC Daresbury Synchrotron Radiation Source using beamlines 16.1 or 2.1 and using image plates or a 2D multiwire proportional detector. In all patterns the strong equatorial reflections (E) have been attenuated artificially by a horizontal strip. The intensities have been folded across quadrants and multiplied by the distance from the centre of the patterns to enhance the outer intensity features. Myosin layer-line orders of the 42.9 nm axial spacing are indicated on the right. **(a)** Relaxed muscle, **(b)** Fully active muscle - the steady state at the plateau of a tetanic contraction, **(c)** Skinned fish muscle in BDM rigor and **(d)** skinned rigor muscle as in (c) but labelled with exogenous myosin heads (S1). The lines in (c) indicate the characteristic 'rigor' layer-line intensities (orders of 72 nm) which are not expected or seen (e.g as in (d)) if the myosin heads label actin filaments uniformly on the actin filament helix. (c) is characteristic of a specific labelling pattern of myosin heads on actin in rigor muscle (Squire & Harford, 1988).

What is clear from a comparison of low-angle diffraction patterns from resting muscle (Figure 2(a)) and muscles with many heads bound to actin (Figures 2(c,d)) is that in the latter cases the actin layer-lines very clearly have enhanced intensity. However, the diffraction patterns from rigor muscle (Figure 2(c)) and from S1-labelled muscle (Figure 2(d)) are very clearly different. The S1-labelled

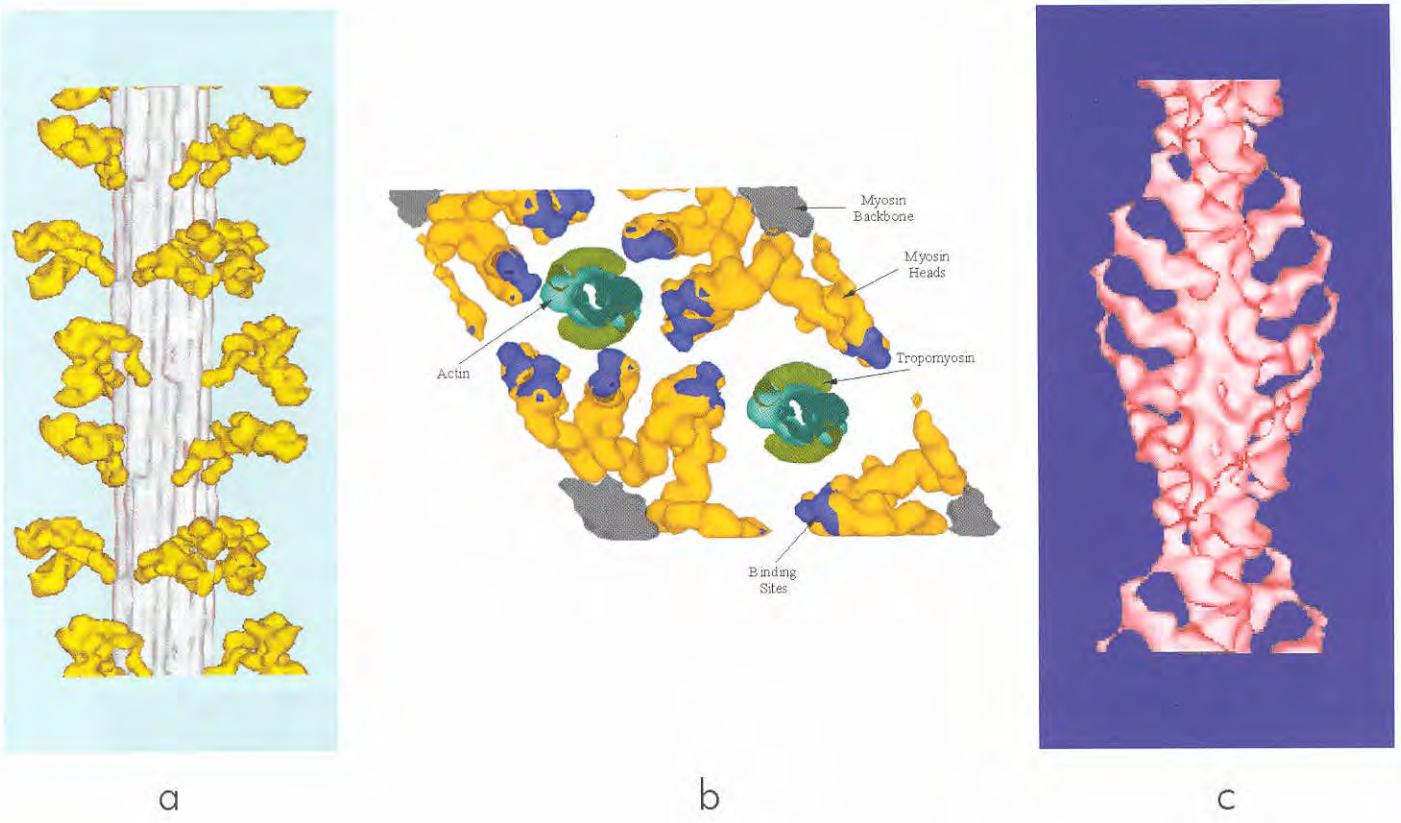

Figure 3: **(a)** Optimised myosin head arrangement in resting plaice fin muscle as determined by Hudson *et al.* [11]. This structure (myosin heads yellow) agrees with the intensities in diffraction patterns such as that in Figure 2(a) with an R-factor of 3%; considerably better than any alternative structures. The figure shows about seven levels of myosin heads spaced at 14.3 nm axial intervals. The observed myosin head axial repeat is three times this at 42.9 nm. **(b)** Four unit cells of plaice fin muscle in the resting state including the myosin filament structure in (a). The grey patches at the corners of the unit cell are the myosin rod assemblies forming the backbones of the thick filaments. The myosin heads (yellow) are on the surface of these backbones. The green, ring-like structures represent actin-tropomyosin filaments in end-on view. The refinement used to model the X-ray diffraction data in Figure 2(a), also refined the absolute orientation of the myosin filament structure in the unit cell. The dark blue patches on the myosin heads represent the actin-binding regions of myosin. Many of these regions are very close to potential binding sites on actin, and stereospecific binding to actin will occur (e.g. in rigor muscle) provided the actin monomer azimuth is suitable for head attachment. It is this that creates the specific non-helical pattern of actin filament labelling that occurs in rigor muscle (Figure 2(c)). **(c)** 3-D helical reconstruction of S1-labelled actin using layer-line intensities from X-ray diffraction patterns such as Figure 2(d) and phases from electron microscopy of decorated actin filaments. The actin filament can be seen as the knobbly strand running up the centre of the figure with the tadpole-like myosin heads attached to it. The axial crossover repeat (near the top and bottom of the figure) is about 36 nm. See Harford *et al.* (1998).

muscle gives a pattern of intensities where the intensity peaks vary in radial position depending on which actin layer-line is involved. The observed diffraction pattern shows characteristic features of actin filaments helically-labelled with myosin heads, giving a helix-cross pattern of intensity. On the other hand rigor fish muscle gives layer-lines (Figure 2(c)) where the peak intensities are all at rather similar radial positions indicating more of a ladder of extra mass labelling the actin filaments. This is entirely consistent with previous analysis which has shown that rigor muscle has myosin heads organised into particular labelling patterns on actin; only azimuthally preferred actin monomers in 'target sites' are being labelled [17].

Myosin Heads with and without ADP

In the most recent study, we have tested whether there is any structural difference between (i) myosin heads in the rigor conformation with no bound nucleotide (Figure 4 left; cf Figure 2(c) which shows the inner part of a similar pattern) and (ii) in the biochemical state where the heads are labelled with ADP (Figure 4: right). Previous studies by electron microscopy and 3D reconstruction of actin filaments labelled with smooth muscle or non-muscle myosin heads [e.g. 18] have suggested that in those cases ADP produces a large conformational change in the myosin heads. However, judging from the results in Figure 4, there are only small structural differences

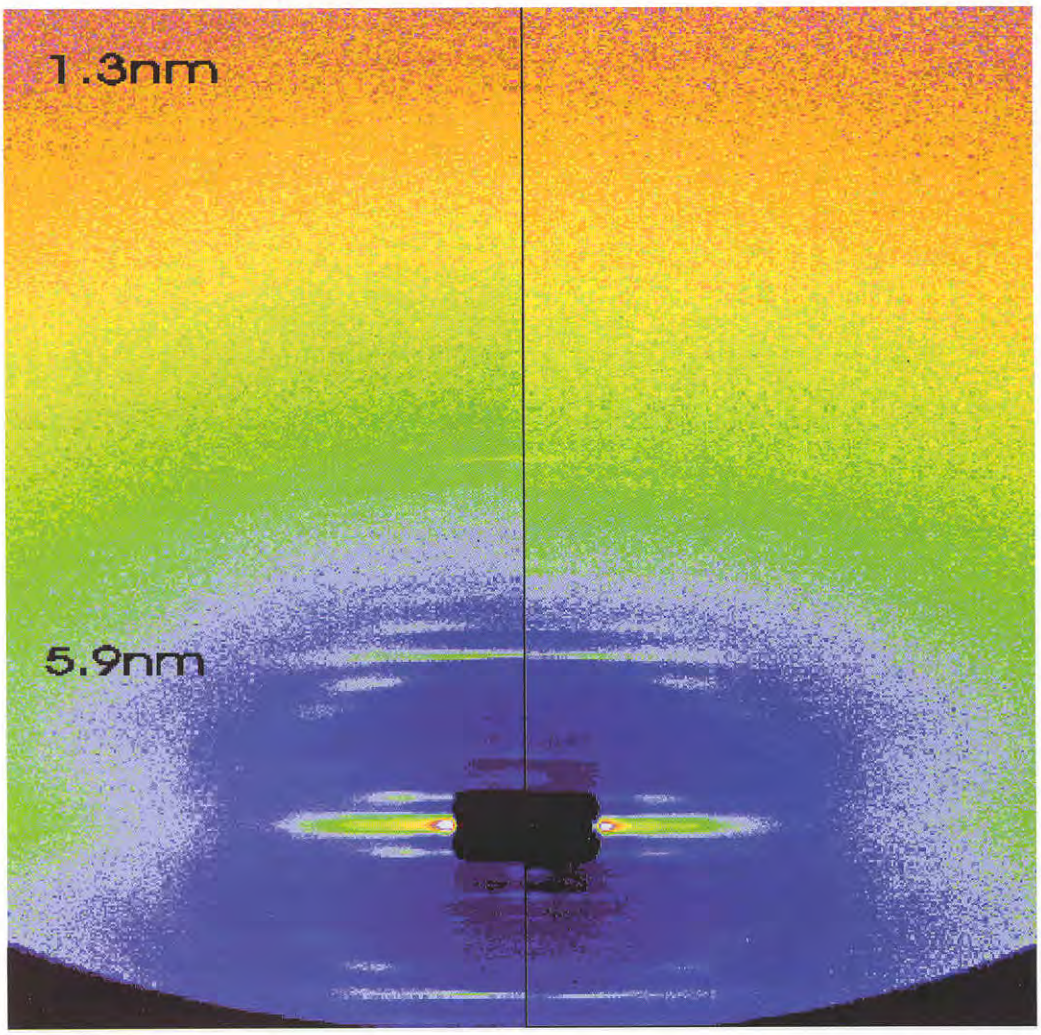

Figure 4: Diffraction patterns from skinned fish muscle in the rigor state showing actin layer-lines out to about 1.3 nm. The patterns were recorded using an image plate and 1.5 m camera length on line 16.1 at Daresbury. The right half of the pattern was from a muscle with ADP present, the left half from the same muscle without ADP. There appear to be only small structural differences between the two states.

between the skeletal muscle myosin head conformation in the presence and absence of ADP. The weak intensity of the layer lines at about 1nm possibly arises due to disordering of the myosin heads in the presence of ADP. This suggests that if any head shape changes occur in the contractile cycle of myosin heads on actin in vertebrate skeletal muscle, they are mainly on phosphate release between the states AM.ADP.Pi and AM.ADP (Figure 1(b)), rather than on ADP release between AM.ADP and AM (rigor). Previous time-resolved X-ray diffraction results on fish muscle have suggested the presence of two structurally different myosin head states on actin in active muscle [2,10,11]. These have been characterised as an initial non-force-producing (weak-binding) state, probably AM.ADP.Pi, and a subsequent force-producing (strong binding) state, probably a combination of AM.ADP and AM. Recent protein crystallography results on smooth muscle myosin [6] have suggested what the structures of two different myosin conformations may be.

Conclusions

The various diffraction patterns show clearly distinct intensity distributions: quasi-helical myosin head arrays on the myosin filament backbone in relaxed muscle (Figure 2(a)), quasi-helical arrays of myosin heads on actin in S1-labelled muscle (Figure 2(d)), head labelling of actin in distinct non-helical, ladder-like, patterns in rigor muscle (Figure 2(c)) and a mixed population of myosin heads on actin in active muscle (Figure 2(b)). There is only a small effect of ADP on the structure of skeletal muscle myosin heads on actin in rigor muscle. With the aid of CCP13 software and our own in-house modelling programs [4,8,10,11], these various states are being solved to define the changing myosin head arrangements between states and especially to determine the structural changes involved in force production and muscle shortening.

Acknowledgements

We acknowledge with appreciation the unfailing support of the non-crystalline diffraction group (particularly Dr. E. Towns-Andrews and Mrs. Sue Slawson) and the detector group (particularly Dr. R. Lewis) at the Daresbury Synchrotron Radiation Source. This work has been supported by the BBSRC, the MRC, the Wellcome Trust and the British Heart Foundation.

References

[1] Harford, J.J. and Squire, J.M., *Biophys. J.* (1996) **50**, 145-155.
[2] Harford, J.J. and Squire, J.M., *Biophys. J.* (1992) **63**, 387-396.
[3] Hudson, L., PhD Thesis (1996), University of London.
[4] Hudson, L., Harford, J.J., Denny, R.C. and Squire, J.M., *J. Mol. Biol.* **273**, 440-455.
[5] Rayment, I., *et al.*, *Science* (1993) **261**, 50-58.
[6] Dominguez, R., Freyzon, Y., Trybus, K.M. and Cohen, C., *Cell* (1998) **94**, 559-571.
[7] Kabsch, K., Mannherz, H.G., Suck, D., Pai, E.F. and Holmes, K.C., *Nature* (1990) **347**, 37-44.
[8] http://www.dl.ac.uk/SRS/CCP13
[9] Squire, J.M., *Curr. Opin. Struct. Biol.* (1997) **7**, 247-257.
[10] Harford, J.J. and Squire, J.M., *Rep. Prog. Phys.* (1997) **60**, 1723-1787.
[11]Harford, J.J., *et al.* and Squire, J.M., in *Proceedings of Hakone Muscle Symposium* (Eds Sugi and Pollack) (Plenum Press, 1998).
[12] Squire, J.M., in *Current Methods in Muscle Physiology* (Ed. H. Sugi) (Oxford University Press, 1998) **241-285**.
[13] Irving, M., *et al.*, *Nature* (1995) **375**, 688-691.
[14] Dobbie, I., *et al.*, and Irving, M., *Nature* (1998) **396**, 383-387.
[15] Reedy, M.K., *J. Mol. Biol.* (1968) **31**, 155-176.
[16] Hudson, L., Denny, R.C., Harford, J.J., Reedy, M.K., Irving, T.C. and Squire, J.M. (in preparation).
[17] Squire, J.M. and Harford, J.J., *J. Mus. Res. Cell Motil.* (1988) **9**, 344-358.
[18] Whittaker, M., Wilson-Kubalek, E.M., Smith, J.E., Faust, L., Milligan, R.A. and Sweeney, H.L., *Nature* (1995) **378**, 748-751.

Microphase separation in Poly(oxyethylene)-Poly(oxybutylene) Diblock copolymers

S.M. Mai[1], J.P.A. Fairclough[2], N.J. Terrill[3], S.C. Turner[2], I.W. Hamley[4], M.W. Matsen[5], A.J. Ryan[2,3] and C. Booth[1]

1 Department of Chemistry, University of Manchester, Manchester, M13 9PL, U.K.
2 Department of Chemistry, University of Sheffield, Sheffield, S3 7HF, U.K.
3 CLRC Daresbury Laboratory, Daresbury, Warrington, Cheshire WA4 4AD, U.K.
4 School of Chemistry, University of Leeds, Leeds, LS2 9JT, U.K.
5 Polymer Science Centre, University of Reading, Whiteknights, Reading, RG6 6AF, U.K.

Introduction

Diblock copolymers with narrow block length distributions may be readily prepared by sequential anionic polymerisation of ethylene oxide followed by 1,2-butylene oxide. We denote these copolymers E_mB_n, where E represents an oxyethylene unit $[OCH_2CH_2]$ and B an oxybutylene unit $[OCH_2CH(CH_2CH_3)]$. Their bulk properties are of significant interest, since microphase-separated structures may form from the disordered melt when the temperature is lowered, either by crystallisation of the E blocks[1-3], or by microphase separation in the melt state[4].

Experimental Procedure

Diblock copolymers were prepared by sequential anionic polymerisation of ethylene oxide (EO) followed by 1,2-butylene oxide (BO). Details of the methods have been published[4]. Characterisation of the intermediate poly(oxyethylene) and the final copolymer was by gel permeation chromatography (GPC) and ^{13}C NMR spectroscopy.

Time Resolved Small-Angle X-Ray Scattering

SAXS measurements were carried out on Beamline 8.2 of the SRS, Daresbury Laboratory, Warrington, UK[6]. The loaded pans were placed in the cell of a Linkam DSC of single-pan design. Samples were heated from room temperature to T_{ODT} + 30 °C at 10 °C min^{-1}, held at the maximum temperature for 1 min

and cooled at 10 °C min^{-1} to 10 °C. The data acquisition system had a time-frame generator which collected the data in 6 s frames separated by a wait-time of 10 μs.

Microphase Structures and Order-Disorder Transition Temperatures

Figures 1 and 2 show SAXS patterns from copolymer melts which illustrate the cubic phase with Im3m symmetry (body-centred cubic, bcc) of copolymer $E_{40}B_{79}$ at 35 °C and the bicontinuous cubic phase with Ia3d symmetry (gyroid, gyr) of copolymer $E_{75}B_{54}$ at 70 °C. The data are presented as log(intensity) versus normalized wave vector, q/q*, where q* is the value of q at the peak of the first-order reflection.

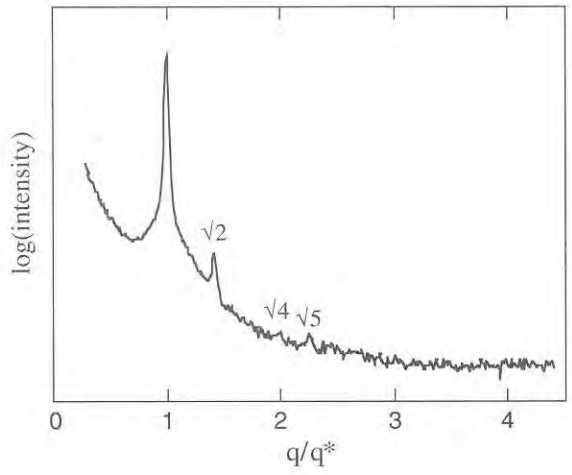

Figure 1: SAXS patterns for the molten copolymer $E_{40}B_{79}$ at 35 °C. q* is the value of q at the peak of the first order reflection. The logarithmic intensity scale is arbitrary. Reflections at q/q* = 1, √2, √4 and √5 indicate a body-centred cubic phase.

Figure 3 shows a time-resolved SAXS schematic of the phase behaviour of copolymer $E_{75}B_{54}$ obtained during heating and cooling the copolymer. At low temperature there are four equally spaced reflections which is consistent with a lamellar semicrystalline phase, at intermediate temperatures (63 °C - 126 °C) the gyroid phase is observed (see Figure 2), while the broad scattering peak at high temperatures (T > 126 °C) indicates a disordered melt with composition fluctuations. The phase sequence is reversed on cooling. Heating and cooling experiments, such as illustrated in Figure 3, were used to locate the temperature of the order-disorder transition (ODT). In fact, as described previously[4], the ODT was defined not only from the step change in the peak-maximum intensity (see Figure 3), but also from the step changes in peak width and peak shape.

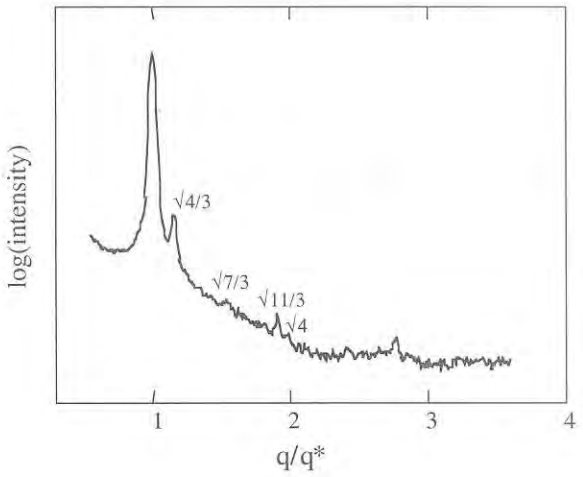

Figure 2: SAXS patterns for the molten copolymer E75B54 at 70 °C. q* is the value of q at the peak of the first order reflection. The logarithmic intensity scale is arbitrary. Reflections at q/q* = 1, ÷4/3, ÷7/3, ÷11/3 and ÷12/3 indicate a gyroid phase.

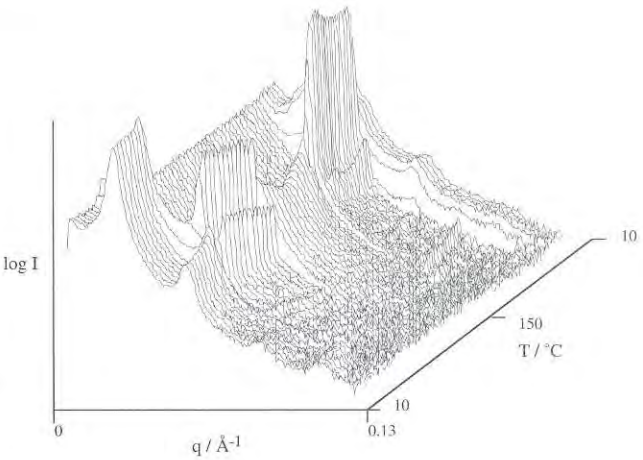

Figure 3: Three-dimensional relief diagram of time-resolved SAXS data obtained with a time resolution of 6 s while heating and cooling copolymer $E_{75}B_{54}$. The plot shows log(intensity) *versus* scattering vector, q, *versus* temperature, T. The thermal cycle was 10°C→150°C→10°C at a ramp rate of 10°C min^{-1}.

Temperature dependence of χ

To locate the copolymers on the conventional phase diagram (χN_v versus ϕ_E), the value of χ is formulated using the accumulated data for symmetrical copolymers (ϕ_E =0.5) as a function of temperature χ=B/T+A. The approximation for χ was evaluated from the mean-field approximation for its critical value (χN_v = 10.5) for microphase separation produced by Leibler[7], which gives

$$\chi = 48.0/T - 0.0535$$

The value of χ was also evaluated using the fluctuation correction by Fredrickson and Helfand[8] (Figure 4)

$$\chi N_v = 10.5 + 41N^{-1/3},\ N = r_v b^6 \rho^2$$

with approximate values for the statistical segment length ($b \approx 5.3 \times 10^{-10}$ m) and number density ($\rho \approx 1.4 \times 10^{28}$ m^{-3}), which gives

$$\chi = 75.6/T - 0.0929$$

Phase Diagram

The results from the samples were used to define the phase boundaries shown in Figure 4, which is plotted with χ calculated for the fluctuating melt. The filled circles denote order-disorder transitions (ODT) while the open circles signify order-order transitions (OOT). With an increase in χN_v (i.e., on cooling) and with the exception of the gyroid phase, all structured phases persisted to the crystal-liquid boundary. Lines are drawn on the phase diagram in order to highlight the features.

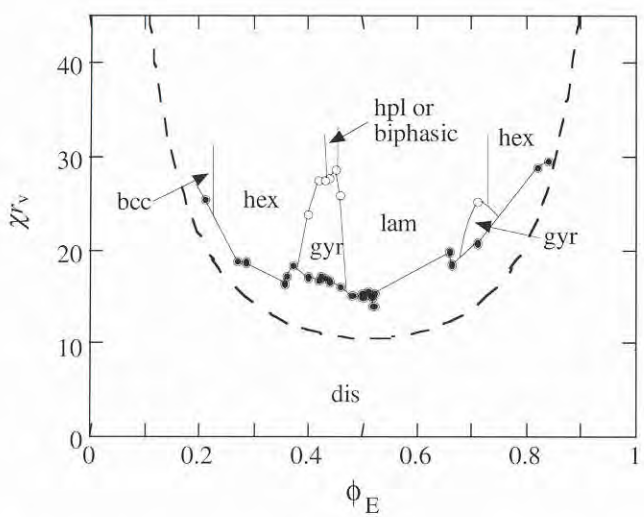

Figure 4: Phase diagram (χr_v *versus* ϕ_E) constructed using χ calculated for the fluctuating melt. The filled circles denote order-disorder transitions (ODT) and the open circles order-order transitions (OOT). The solid curves have been drawn to indicate the different phases observed, but do not correspond to precise phase boundaries. The dashed curve is the boundary predicted by self-consistent mean-field theory.

The phase diagram is asymmetric about $\phi_E = 0.5$. If χ is independent of ϕ_E, the global symmetry of the phase diagram is controlled by the conformational asymmetry parameter, ε, where

$$\varepsilon = (v_E b_B^2 / v_B b_E^2)$$

where v_E, v_B, b_E and b_B represent the volumes and statistical lengths of the E and B blocks. Only if $\varepsilon = 1$ can the phase diagram be symmetrical. For this E/B system $\varepsilon = 0.65$[1,4] and this effect is to bias the phase diagram to the high ϕ_E side.

Figure 4 shows that the ODT boundary is not smooth, particularly between the disordered and gyroid phase which occurs at a higher χN_v than would be required for a smooth boundary between the lamellar and hexagonal regions. This reflects the lower ODT temperature observed for the gyroid phase than the lamellar or hexagonal phase formed from a copolymer with the same segment length. Figure 4 also shows the theoretical predictions (dashes) predicted by self-consistent field theory[7,9,10]. Theory predicts $\chi N_v = 10.5$ at $\phi_E = 0.5$ compared with $\chi N_v = 14$ for the experimental boundary. Mean-field theory has not yet been generalized to account for composition fluctuations. However, the difference between experiment and theory is in part forced because allowance was made for a fluctuating melt when treating experimental data to calculate χ.

References

[1] Yang, Y.-W., Tanodekaew, S., Mai, S.-M., Booth, C, Ryan, A. J., Bras, W. and Viras, K., *Macromolecules* (1995), **28**, 6029.

[2] Ryan, A. J., Fairclough, J. P. A., Hamley, I. W., Mai, S.-M. and Booth, C., *Macromolecules* (1997), **30**, 1723.

[3] Mai, S.-M., Fairclough, J. P. A., Viras, K., Gorry, P. A., Hamley, I. W., Ryan, A. J. and Booth, C., *Macromolecules* (1997), **30**, 8392.

[4] Mai, S.-M., Fairclough, J. P. A., Hamley, I. W., Matsen, M. W., Denny, R.C., Liao, B.-X., Booth, C. and Ryan, A. J., *Macromolecules* (1996) **29**, 6212.

[5] Bras, W., Derbyshire, G. E., Ryan, A. J., Mant, G.R., Felton, A., Lewis, R.A., Hall, C.J. and Greaves, G.N., *Nuclear Instruments and Methods in Physics Research* (1993) **A326**, 587.

[6] Bras, W., Derbyshire, G. E., Clarke, S., Devine, A., Komanschek, B. U., Cooke, J. and Ryan, A.J., *J. Appl. Cryst.* (1994), **35**, 4537.

[7] Leibler, L., *Macromolecules* (1980) **13**, 1602.

[8] Fredrickson, G.H. and Helfand, E., *J. Chem. Phys.* (1987) **87**, 697.

[9] Matsen, M.W. and Schick, M., *Phys. Rev, Lett.* (1994) **72**, 2660.

[10] Matsen, M.W. and Bates, F.S., *Macromolecules* (1996) **29**, 1091.

Effect of Shear on Block Copolymer Gels

I.W.Hamley[1], J.A.Pople[1], C.Booth[2], J.P.A.Fairclough[3], A.J.Ryan[3,4], N.J.Terrill[3,4], G.P.Diakun[4], A.J.Gleeson[4], B.U.Komanschek[4], S.M.King[5], K.Almdal[6] and K.Mortensen[6] and O.Diat[7]

1 School of Chemistry, University of Leeds.
2 Department of Chemistry, University of Manchester.
3 Department of Chemistry, University of Sheffield.
4 CLRC Daresbury Laboratory, Daresbury.
5 CLRC Rutherford Appleton Lab, Chilton, Didcot.
6 Dept. of Condensed Matter Physics, Risø National Lab, Denmark.
7 ESRF, France.

We have recently been investigating the effect of shear on lyotropic liquid crystalline phases formed by amphiphilic block copolymers. The particular focus has been on poly(oxyethylene)-poly(oxybutylene) diblock copolymers in aqueous solutions. We have constructed a facility for simultaneous SAXS and rheology, based on a modified commercial Rheometrics RSA II rheometer and this will be described. We have successfully demonstrated this instrument at the SRS, Daresbury Laboratory, UK [1]. A similar instrument has recently been installed at the SANS beamline at Risø National Laboratory, and we have also performed collaborative research there [2,3]. In addition, we have performed experiments using the Couette cell on BL4 at the ESRF where the effect of steady shear on ordered mesophases in block copolymer solutions was examined [3,4]. Shearing experiments at the SANS instrument at ISIS, U.K. have yielded additional information on the effect of high rates of steady shear [5]. Finally, we have recently constructed a highly flexible Couette cell for steady or oscillatory shear for use at the SRS (SAXS) and the ISIS (SANS) and this will be described. Selected results from all these experiments will be discussed. In particular (i) The effect of steady and oscillatory shear on generating macroscopically oriented cubic "crystals" of block copolymer gels, of bcc and fcc symmetry [1,3-5], (ii) The quantitative analysis of the extent of orientation of a hexagonal-packed cylindrical micellar phase and time-resolved studies of the orientation process [6], and (iii) The influence of shear on the orientation and domain spacing of a lamellar phase formed by an amphiphilic block copolymer in solution [7]. This includes the intriguing obervation of a shear-induced reduction in domain spacing.

References

[1] Pople, J.A., Hamley, I.W., Fairclough, J.P.A., Ryan, A.J., Yu, G.-E. and Booth, C., *Macromolecules* (1997) **30**, 5721.
[2] Vigild, M.E., Almdal, K., Mortensen, K., Hamley, I.W., Fairclough, J.P.A. and Ryan, A.J., *Macromolecules* (1998) **31**, 5702.
[3] Hamley, I.W., Pople, J.A., Fairclough, J.P.A., Terrill, N.J., Ryan, A.J., Booth, C., Yu, G.-E., Diat, O., Almdal, K., Mortensen, K. and Vigild, M., *J. Chem. Phys.* (1998) **108**, 6929.
[4] Hamley, I.W., Pople, J.A. and Diat, O., *Colloid Polym. Sci.* (1998) **276**, 446.
[5] Hamley, I.W., Booth, C., Yang, Y.-W. and King, S.M., *Langmuir* (1998) **14**, 3182..
[6] Pople, J.A., Hamley, I.W., Terrill, N.J., Fairclough, J.P.A., Ryan, A.J., Yu, G.E. and Booth, C., *Polymer* (1998) **39**, 4891.
[7] Pople, J.A., Hamley, I.W. and Diakun, G.P., *Rev. Sci. Instrum.* (1998) **69**, 3015.

Structural Transition in Hydrogel-Drug Systems

B.Y. Shekunov[1], P. Taylor[2] and J.G. Grossmann[3]

1 Drug Delivery Group, Postgraduate Studies in Pharmaceutical Technology, School of Pharmacy, University of Bradford, Bradford BD7 1DP, UK.
2 Department of Pharmaceutical Sciences, De Montfort University, The Gateway, Leicester LE1 9BH, UK.
3 Daresbury Laboratory, Daresbury, Warrington, Cheshire WA4 4AD, UK.

This study aimed to investigate structural ordering/transition phenomena in a cross-linked poly(ethylene oxide) 4000 (PEO) matrix which is saturated with an active compound (paracetamol or caffeine) and used as a model drug delivery system. Time-resolved small angle X-ray scattering (SAXS) and wide angle X-ray scattering (WAXS) measurements were carried out using the synchrotron radiation source at Daresbury

Laboratory. The experiment consisted of, first, studies of PEO recrystallization at different degrees of hydration in the gel and, second, formation and dissolution of fine particulate drug materials within the hydrogel matrix. Other analytical techniques such as small angle neutron scattering, atomic force microscopy and drug dissolution complemented the experimental work. Unhydrated gels show a developed semi-crystalline structure which became more disordered as the hydrogel recrystallized. There is an indication of a kinetic ripening in the crystalline phase. The lamellar structure undergoes transition at 20-40% of water uptake in which the lamellar spacing decreases more than twice with increasing water content. This effect is attributed to the ordered hydrophobic/hydrophilic regions in the gel. Drug-loaded hydrogels exhibit a significant interaction between the polymer and drug molecules, for example, caffeine forms crystalline particles whereas paracetamol remains in an amorphous state likely forming molecular complexes with the polymer. This difference is explained on the basis of specific hydrogen bonding within the polymer matrix. Drug concentrations as small as 1 wt% have a pronounced effect on the mechanical and drug-release properties the hydrogel.

Important Steps in the Analysis of X-ray Scattering and Fibre Diffraction Area Detector Data

A.P. Hammersley

ESRF, BP 220, 38043 Grenoble, France.

Area detectors are indispensible for efficient data collection for many types of experiment, but they are far from perfect and introduce various distortions into the data. For accurate analysis and interpretation of such data, characterisation of detector distortions and correction prior to further analysis is vital. For scattering data this particularly means that very careful attention must be paid to effects which distort intensities, as final intensities must be linear over a very wide dynamic range, and as a function of both detector position and angle of incidence. For fibre diffraction data, intensity accuracy is of lesser importance, but positional accuracy is of much greater importance. The effects which can lead to these distortions will be discussed as will the calibration techniques necessary to quantify and correct them. The manner in which the integration of 2-D regions from a variety of 1-D and multiple 1-D scans is performed is very important. In order to obtain accurate intensities a variety of geometrical effects, and the effect of polarisation on the intensities, must be accounted for during integration. Algorithms to perform integration and possible types of output will be discussed. Examples of data analysis and graphical display of results will also be presented.

SANS/WANS Anyone?

S.M. King

ISIS Facility Rutherford Appleton Laboratory Chilton DIDCOT OX11 0QX UK.

Simultaneous SAXS/WAXS has become a highly-regarded technique for the study of soft condensed matter, particularly polymers. The complementary technique with neutron radiation has however been slower to develop. Late 1997 saw the culmination of an SERC funded upgrade to the "white-beam", "fixed-geometry", time-of-flight SANS instrument (called "LOQ") at ISIS. The upgrade has more than quadrupled the available Q-range, now 0.008-1.4$Å^{-1}$, all of which is accessible - with full azimuthal coverage - in a single measurement without the need for any reconfiguration of the instrument. This talk will describe the nature of the upgrade, some early results, and the opportunities that exist for Non-Crystalline Diffraction at ISIS.

Thin film studies of diblock copolymers on 16.2

J.P.A. Fairclough[1], A.J.Ryan[1,2], C. Salou[1], S-M. Mai[3], C. Booth[5], I.W. Hamley[4], J.A. Pople[4] and G. Clark[2]

1 Department of Chemistry, University of Sheffield, Sheffield, S3 7HF.
2 CCLRC, Daresbury Laboratory, Daresbury.
3 Department of Chemistry, University of Manchester.
4 Department of Chemistry, Universityof Leeds, Leeds, LS2 9JT.

Thin films of block copolymers can be cast onto surfaces by various means. Spin casting forms a thin coating, which is dependent on the concentration, and spin speed. On application, the copolymer

molecules are trapped in non-equilibrium structures. These structures can be annealed into equilibrium structures over a period of a few hours. The surface of the substrate may be selective for one block. If this is the case then the blocks tend to segregate and stack in alternating layers on the surface. We have used reflectivity and Grazing Incidence Diffraction to study the self-assembly of these layers in a range of materials. We have shown that the stems of short crystalline block copolymers selective for the substrate surface align perpendicular to the surface, without tilting as was previously assumed.

X-PLOR for Polycrystalline Fibre Diffraction

R.C. Denny

CLRC Daresbury Laboratory.

The X-PLOR system [1] for NMR and protein crystallography is a flexible software package which allows molecular structures to be investigated. Among other things, the package allows a chosen target function to be used as an empirical X-ray energy term which can be added to the potential energy of a molecule. Techniques such as energy minimization and simulated annealing can then be applied to ensure reasonable stereochemistry and an optimal fit to the X-ray data.

Wang & Stubbs [2] have addressed the problem of applying X-PLOR to filamentous viruses which give rise to unsampled layer-lines of intensity and are constrained by a high degree of non-crystallographic symmetry. Further modification to some X-PLOR routines has been necessary to allow covalent bonding between symmetry related portions of molecular structure and to treat the systematically overlapping but not symmetrically related reflections common in diffraction patterns of polycrystalline fibres.

These modifications and some trial applications of the modified program will be discussed.

References

[1] Brunger, A.T., Kuriyan, J. and Karplus, M., *Science* (1987) **235**, 458-460.

[2] Wang, H. and Stubbs, G., *Acta Cryst.* (1993) **A49**, 504-513.

End Functionalised Polymers Grafted To An Interface

R.W. Richards and H.L. Thompson

IRC in Polymer Science and Technology, University of Durham, DURHAM, DH1 3LE.

At sufficiently high number of polymer molecules per unit area (grafting density), polymers attached by their ends to a planar surface form a 'brush' like layer where the molecules stretch in a direction normal to the interface. In addition to the grafting density, the characteristics of the brush like layer, i.e. the surface volume fraction, the surface excess and the brush height (or layer thickness) are also controlled by the nature of the surrounding matrix. The two extremes are a stretched 'wet' brush when the matrix is a low molecular weight thermodynamically favourable solvent and a 'dry' brush when the matrix has a molecular weight greater than or equal to the grafted polymer. A 'phase diagram' of relationships for the brush height has been proposed. Moreover such grafted polymer layers are also susceptible to analysis by mean field methods enabling the 'sticking' energy of the attaching species to be evaluated.

Reflectometry is an aspect of small angle scattering using neutron beams that has been developed in the last 8-10 years. The scattering vector is normal to the surface on which the beam is incident and thus the characteristics of grafted layers can be obtained if use is made of selective deuteration. An outline of the principles will be presented and the importance of using confirmatory data, where obtainable, will be stressed. Attention will be focussed on mixtures of deuteropolystyrene functionalised at both ends (molecular weight ~ 100,000) mixed with hydrogenous polystyrene matrices with a range of molecular weights (52,000 to $1x10^6$). We show that the near surface depth profiles are narrower than those for the same polymer functionalised at one end only as predicted by theory. However, contrary to expectations based on the grafting density and the molecular weights of the matrices, the brush height (and other parameters) exhibits stretched wet brush behaviour. Sticking energies evaluated from a mean field theory will also be presented.

Interplay of solution scattering, crystallography and 3D modelling of proteins

J.G. Grossmann[1], Q. Hao[2], F.E. Dodd[1] and S.S. Hasnain[1]

1 CCLRC Daresbury Laboratory, Warrington WA4 4AD, U.K.
2 Department of Chemistry and Physics, De Montfort University, Leicester LE1 9BH, U.K.

X-ray scattering is a very effective technique for obtaining low-resolution structural details of proteins and their complexes in solution. Recently, there has been significant progress with the development of an ab initio method for shape restoration in terms of spherical harmonics from scattering data [Svergun & Stuhrmann (1991) *Acta Cryst.* **A47**, 736-744]. Crystallographic data clearly contain more information and provide much higher resolution. However, solving the phase problem is the crucial and quite often the most difficult and time consuming step in crystallographic structure determination. The traditional methods of isomorphous replacement or molecular replacement require the availability of isomorphous heavy atom derivatives or the structure of a homologous protein, respectively. Here we demonstrate that the low-resolution molecular shape determined from solution X-ray scattering data can be located in the crystallographic unit cell using experimental diffraction data. It is anticipated that the low-resolution molecular envelope can be used as a starting model for phase extension by maximum entropy and density modification methods. Protein crystals are a prerequisit for high-resolution structure determination. Let us assume the specific case where suitable crystals are lacking, no noticeable sequence homology to any other structurally chracterized protein is available, but a molecular shape has been determined from solution scattering data. This scenario has been investigated in order to evaluate the possibility of using solution scattering in conjunction with biochemical information and structure prediction techniques for protein modelling. Results will be presented and discussed.

Developments to Sample Environments within NCD

N.J. Terrill

CLRC, Daresbury Laboratory, Warrington, WA4 4AD.

Developments in the Sample Environment portfolio of NCD will be discussed, including designs for a new automatic sample changer and a pressure cell together with the possibilities for magnetic studies on the NCD Stations. This is also an opportunity to discuss the direction that we want to take where sample environment is concerned. Station 16.2 has been incorporated into the NCD group as of April 1st 1998. The station will also be described and its modes of operation investigated. Station 16.2 has been designed and constructed to study the structure of surfaces and interfaces. It is configured as a 6-circle, horizontal diffractometer and vertical reflectometer. The diffractometer is equipped with an analyser stage and therefore has triple axis capabilities.

The DUBBLE SAXS/WAXS Beamline

W. Bras

ESRF, BP 220, 38043 Grenoble, France.

A new ESRF beamline, built by a Dutch/Belgian consortium and dedicated to combined time resolved SAXS/WAXS and fibre diffraction experiments, will be described. The expected performance, the problems encountered and the ones to be expected will be discussed.

A major problem will be in detectors that can handle the extremely high count rates that can be generated by beamlines on third generation sources. Therefore we have developed a new type of detector with a relatively high count rate capability. This detector is based on well known technology already widely used in high energy physics experiments but in order to use this technology a new electronic system had to be designed.

Some other experimental problems that can be encountered will be mentioned as well.

The Crystal Structure of Poly(ethylene terephthalate) Revisited

K.H. Gardner[1] and D.L. Dorset[2]

1 Dupont CR&D, Wilmington, DE, USA.
2 Hauptman-Woodward Medical Research Institute, Inc., Buffalo, NY, USA.

In 1954, Daubeny, Bunn and Brown, reported the first determination of the structure of poly(ethylene terephthalate) [1]. With the wealth of new technology, we have decided to revisit this polymer. A data set from a PET monofilament has been collected using an image plate (APS, 0.100nm radiation) and a powder diffractometer (symmetrical transmission, 0.1.54nm radiation). The diffraction data has been processed using XDPP and a data set consisting of the positions and intensities of ~80 reflections were determined. The structure has been determined by direct methods and by LALS refinement. The methodology and results will be discussed.

References

[1] Daubeny, R.deP., Bunn, C.W. and Brown, C.J., *Proc. Roy. Soc. (London)* (1954) **A226**, 531.

First Beamline Results from the RAPID system

R.A. Lewis, A. Berry, N.S. Fore, C.J. Hall, A.O. Jones, W.I. Helsby and B.Parker

CLRC Daresbury Laboratory.

Multiwire proportional counters have been used for many years to capture X-ray images from synchrotron sources. They are particularly well suited to dynamic experiments and have time resolutions of the order of microseconds. They are almost noise free, have high dynamic range and large active areas. However, they do have limitations in the global and local count rate performance. RAPID, the Refined ADC per Input Detector, is a two dimensional detector system which delivers a more than twenty fold increase in throughput over present systems on the SRS. It comprises a wire micro-gap detector and a sophisticated multi channel data acquisition system. RAPID has a global count rate limit of greater than 30 million photons per second and a maximum local rate limit of of greater than 1 million photons per square millimeter. The system has shown spatial resolutions of 250 microns (FWHM) and has a 200 mm by 200 mm active area. The performance of the detector and readout system during its first 'user' tests will be presented.

Neutron Fibre Diffraction Studies on Instrument D19 at the Institut Laue-Langevin

V.T. Forsyth[1], M.W. Shotton[1], L.H. Pope[1], H. Ye[1], C. Boote[1], P. Langan[2], R.C. Denny[3] and W. Fuller[1]

1 Physics Department, Keele University, Staffordshire, ST5 5BG, England.
2 Institut Laue Langevin, Avenue des Martyrs, Grenoble, France.
3 Blackett Laboratory, Imperial College, London University, England.

Neutron high-angle fibre diffraction techniques offer unique opportunities in structural studies, and can provide information that is difficult or impossible to obtain using X-ray methods. Such techniques can be applied to a wide variety of natural and synthetic polymer systems and are particularly powerful in the study of biological systems in which ordered water plays a central role or where the location of individual hydrogen atoms is important. These methods were used very successfully to study the location of ordered water around different conformations of the DNA double helix, and have subsequently been used by a number of groups in the study of other biological fibrous systems, including cellulose, filamentous viruses, and hyaluronic acid. The main features of neutron diffraction that are exploited in these studies are (i) the fact that the coherent scattering length of hydrogen is greater (in comparison to other atoms) for neutrons than is the case for X-rays and (ii) the fact that deuterium has a strikingly different scattering length from its lighter isotope. Isotopic replacement methods can therefore be used to image particular atoms or molecules within a structure.

The D19 diffractometer at the Institut Laue-Langevin is unquestionably the best instrument in the world for neutron high-angle fibre diffraction experiments. The methods used in sample preparation, data

collection, and data analysis will be discussed, and illustrative examples taken from recent work on DNA.

References

[1] New developments in instrumentation for fibre diffraction experiments, Shotton, M.W., Pope, L.H., Forsyth, V.T., Denny, R.C., Archer, J., Langan, P., Ye, H. and Boote, C., *J. Appl. Cryst.* (1998), **31**, 758-766.

[2] A high-angle neutron fibre diffraction study of the hydration of deuterated A-DNA, Shotton, M.W., Pope, L.H., Forsyth, V.T., Langan, P., Denny, R.C., Giesen, U., Dauvergne, M.-T. and Fuller, W., *Biophysical Chemistry* (1997) 69 (1), 85-96.

Peptide Self-Assembly: A Route to Novel Biopolymers

N. Boden

1 SOMS Centre, The University of Leeds, Leeds LS2 9JT, UK.

In 1994, a research student, Amalia Aggeli, working in the SOMS Centre, made the unexpected observation that a peptide she was making as a model for a transmembrane ion channel, formed a gel in solution. Driven by curiosity, we proceeded to establish that these gels consisted of a network of entangled polymeric beta-sheet tapes, each a single molecule in thickness. What in effect we had stumbled on was a new kind of polymer. These polymers are of especial interest because, firstly, they are produced by biological-like molecular self-assembly, which can be switched on or off by chemical triggers. And, secondly, they are tape-like rather than string-like in structure. This discovery was reported in Nature in 1997 (vol 386, pp 259-262). We have gone on to establish a set of rational design principles for the production of tape-forming peptides and to study their properties in solution and their interaction with surfaces. Under certain conditions the tapes supercoil to form fibrils similar to those encountered in Alzheimers or Parkinsons disease. An overview of this work will be presented.

X-Ray Rheology of Unstructured and Structured Polymer Melts

G.R. Mitchell, E.M. Andresen and P.M.S. Roberts

Department of Physics, University of Reading, Whiteknights, Reading RG6 6AF, U.K.

Time-resolving X-ray scattering measurements performed on samples subjected to shear flow provide both a powerful insight to the structural re-organisation which accompanies flow and an approach to interpret mechanical rheological data. Novel equipment which facilitates such measurements is described and the procedures developed to analyze the scattering patterns are outlined. With this X-ray rheology system we explore the flow behaviour of both structured and unstructured polymer melts. In particular, we show how such procedures may be used to understand the complex flow behaviour of liquid crystal polymer systems. We contrast the development of macroscopic orientation during flow in thermotropic systems with that observed for equivalent lyotropic materials and study the relaxation behaviour following cessation of flow. We compare such behaviour with the much more delicate balance in thermotropic side-chain liquid crystal polymers between the liquid crystal component and the transient polymer network.

In-situ X-ray diffraction study of the effect of flow upon surfactant liquid crystalline phases

A.E. Terry[1], J.A. Odell[1], R.J. Nicol[2], G.J.T. Tiddy[2] and J.E. Wilson[3]

1 H.H. Wills Physics Lab., University of Bristol, Tyndall Ave., Bristol, BS8 1TL.

2 Dept. of Chem. Eng., UMIST, PO Box 88, Manchester, M60 1QD.

3 Unilever Research, Port Sunlight Lab., Quarry Road East, Bebington, Wirral, L63 3JW.

The equilibrium structures of aqueous surfactant liquid crystalline mesophases are mostly well established, as is their dependence on surfactant type. Simple concepts of molecular and micellar size and shape, involving 'packing constraints', have been fundamental to this understanding. Both shear

and extensional flow have a profound effect on the structure and orientation of these complex fluids. Time-resolved X-ray diffraction has been utilised to probe the dynamic response of these mesophases, so that the macroscopic rheological behaviour can be related to the flow-induced structural changes observed. In-situ X-ray diffraction studies will be presented examining the effect of flow upon hexagonal and lamellar surfactant liquid crystalline phases. For each system, significant flow deformation occurred. The interpretation of the rheological behaviour in terms of molecular structure will be discussed and compared to the molecular theories for liquid crystalline flow.

High-temperature BCC lattice formation /disappearance in triblock copolymer gels: morphological transition or order frustration?

R. Kleppinger[1], N. Mischenko[1], L. Theunissen[1], H. Reynaers[1], K. Mortensen[2], K. Almdal[2], M.H.J. Koch[3]

1 Dept. of Chemistry KULeuven, Celestijnenlaan 200F, B-3001 Belgium.
2 Risoe National Laboratory, Denmark.
3 EMBL-Outstation, Germany.

Triblock ABA copolymer gels, based on a three-dimensional physical network of polystyrene-rubber-polystyrene copolymers in a relatively low molar mass (Mw ~ 400-500) solvent selective for the midblock (B), are soft solid materials [1-2]. They have high elasticity and deformability (100 - 1000%), depending on molar mass and block ratio of the copolymer [3-4]. At ambient temperature a short-range ordered arrangement of the network nodes (spherical domains of the endblocks) results in a morphology intermediate between liquid-like and a highly distorted crystalline one [2,5]. For some gels a real polycrystalline (BCC) structure has been observed developing within a certain temperature range [6,7]. However, it tends to disappear beyond these temperature limits. While the existence of the high-temperature limit sounds reasonable, the reason of the low-temperature one is disputable. It is worth mentioning that BCC structure is also reported for micellar solutions of the same triblock copolymer in a different solvent (for instance, in hexane at room temperatures) although they do not have elastic rubber properties.

At ambient temperature, the structure of the network in our gels can be described in terms of a highly distorted crystalline lattice of close-packed spheres (CPS, either HCP or FCC) or in terms of liquid with effective hard-sphere interaction. Therefore two possible mechanisms exist for the low-temperature transformation: frustration of the BCC morphology or a change to a different one. We are going to discuss this matter on the basis of real-time SAXS scans during cooling-heating or isothermal annealing and equilibrium SANS measurements.

References

[1] Mischenko, N., Reynders, K., Mortensen, K., Scherrenberg, R., Fontaine, F., Graulus, R. and Reynaers, H., *Macromolecules* (1994) **27**, 2345-2347.
[2] Mischenko, N., Reynders, K., Koch, M.H.J., Mortensen, K., Pedersen, J.S., Fontaine, F., Graulus, R. and Reynaers, H., *Macromolecules* (1995) **28**, 2054-2062.
[3] Reynders, K., Mischenko, N., Mortensen, K., Overberg, N. and Reynaers, H., *Macromolecules* (1995) **28**, 8699-8701.
[4] Mischenko, N., Reynders, K., Mortensen, K. and Reynaers, H., *J. Polym. Sci. B - Polym. Phys.* (1996) **34**, 2739-2745.
[5] Reynders, K., Mischenko, N., Kleppinger, R., Mortensen, K., Koch, M. and Reynaers, H., *J. Appl. Cryst.* (1997) **30**, 684-689.
[6] Kleppinger, R., Reynders, K., Mischenko, N., Overberhg, N., Koch, M., Mortensen, K. and Reynaers, H., *Macromolecules* (1997) **30**, 7008-7011.
[7] Kleppinger, R., Mischenko, N., Theunissen, E., Koch, M., Almdal, K., Mortensen, K. and Reynaers, H., *Macromolecules* (1997) **30**, 7012-7014.

Better Access for Regular use of Networked Software: B.A.R.N.S

D. Richard and G.J. Kearley

Institut Laue-Langevin, B.P. 156 38042, Grenoble Cedex 9, France.

Although the ILL is in France, more than 70% of the 2000 visits per year are from people outside France, and because their visits are necessarily short, serious

data treatment and analysis usually begins when they return to their home institute. Traditionally, much analysis has been made using remote-access to the ILL, but a number of recent developments have made remote-user access almost useless:
1. Firewalls complicate remote-terminal use.
2. Many programs use X which performs badly over remote connections.
3. Most ILL programs are platform dependent.

The solution is obvious: Create a server at the ILL (we call it BARNS) which allows programs to execute on ILL computers but with input/output via the internet to "standardised" frames and applets within the clients web-browser. This is not simply an exercise in creating an HTML form for each program. BARNS must:
1. Appear multi-user, multi-threaded, and access multiple nodes.
2. Handle all aspects of user login, accounts, processes, zombies etc.
3. Create standardised frames which can handle almost any program requirements with minimum effort.
4. Automatically direct output to the correct frame: program, graphics or tools.

We will show how little modification is necessary in order that programs can run under BARNS and how interactivity is achieved.

Real Time X-Ray Diffraction Studies on the Formation of Intermediates in Phospholipids Induced by Laser T-Jump

G. Pabst[1], M. Rappolt[1], H. Amenitsch[1], S. Bernstorff[2] and P. Laggner[1]

1 Institute of Biophysics and X-ray Structure Research, Austrian Academy of Sciences, Steyrergasse 17, A-8010 Graz, Austria.
2 Sincrotrone Trieste, Experimental Division, SS 14, 163.5 km, I-34012 Basovizza (TS), Italy.

Supramolecular phospholipid aggregates - bilayers - form the matrix of all membranes. Their structural variability confers the characteristics of dynamics to cell membranes which is of utmost functional importance. So far there were no methods existing which would allow the study in real time of these structural dynamics, because they are characterized by relaxation times in the subsecond time domain. Synchrotron radiation with its extremely high X-ray flux has now made this possible. At the Austrian SAXS-Station of the synchrotron radiation light source ELETTRA in Triest, a dedicated experimental facility for such X-ray kinematographic jump relaxation studies has been installed by the IBR. Here is a first report on the detection of short-lived non-equilibrium intermediate structures.

Mammographic imaging using the SRS

R.A. Lewis[1], C.J. Hall[1], W.I. Helsby[1], F. Ortuno-Prados[2], A. Hufton[3] and C.R.M. Boggis[4]

1 CLRC Daresbury Laboratory, Keckwick Lane, Daresbury, Cheshire.
2 Laboratorio del Sincrotron de Barcelona, IFAE Edifici Cn Campus Univ. Autonoma de Barcelona, Spain.
3 North West Medical Physics, Christie Hospital, Withington, Manchester.
4 Nightingale Breast Screening Centre, Manchester.

It has been reported that the use of synchrotron radiation for mammography results in images of higher quality, at lower dose, than those obtained using conventional hospital equipment. A direct comparison of the image quality obtained by conventional and synchrotron based mammographic imaging systems has been performed. The work was carried out at the SRS station 8.4, and the Nightingale Breast Screening Centre, a major regional screening centre in Manchester.

The results of these tests are presented along with some preliminary data on the simultaneous imaging, and diffraction measurements of breast tissue, which can be used to obtain tissue specific images.

Fibre diffraction using the BioCAT undulator beamline at the Advanced Photon Source

T. Irving, B. Fischetti, G. Rosenbaum and G. Bunker

BioCAT, Dept. Biological Chemical and Physical Sciences, Illinois Institute of Technology, Chicago IL. 60616 USA. and SBC-CAT, Argonne National Labs, Argonne IL.

The BioCAT undulator-based beamline at the Advanced Photon Source, Argonne IL, USA, is

designed to be a superb instrument for biological non-crystalline diffraction and X-ray absorption spectroscopy. The optics consist of a vertically focussing mirror and a sagitally focussing second monochromator crystal allowing independent focussing of the beam in the vertical and horizontal direction virtually anywhere in the 12 m experimental enclosure. We have documented a focal spot with a 2 m fibre diffraction camera of less than 40 x 200 microns (FWHM) containing essentially all of the 1.5 - 2.0 $\times$ 10^{13} ph/s delivered by the water cooled Si(111) double crystal monochromator. At the minimum focal distance, a less than 25 micron (FWHM) vertical focal spot has been achieved. Here we present results of fibre diffraction experiments performed during our commissioning activities since first light was achieved in September of 1997. This combination of optics and the very low divergence of the very small source have yielded very high quality patterns from various muscle specimens and collagens from human tissues. Most of these patterns were taken on BAS-V image plates scanned with a FujiBAS2500 image plate scanner. This combination is a significant improvement over earlier models for fibre diffraction work. We have also just taken delivery of a 1k x 1k CCD detector that has been optimized for SAS applications and will be capable of various streak camera modes that can be used for time framing applications. Future developments will include commissioning of a cryogenically cooled monochromator, in vacuum beam monitoring, longer camera lengths (6-8 m), and optimizations to improve first order resolution.

Improved Structural Data on Native Cellulose from Neutron and Synchrotron Fibre Diffraction Diagrams

Y. Nishiyama[1,2], T. Okano[2], H. Chanzy[1] ,P. Langan[3] and C. Riekel[4]

1 CERMAV-CNRS, B.P. 53, 38041 Grenoble Cedex 9, France.
2 Department of Biomaterials Sciences, Graduate School of Agricultural and Life Sciences, The University of Tokyo, Tokyo 113-8654, Japan.
3 Institut Max von Laue - Paul Langevin, B.P. 156, 38042 Grenoble Cedex, France.
4 European Synchrotron Radiation Facility, B.P. 220, 38043 Grenoble Cedex, France.

The current sets of coordinates that are commonly used for the definition of the molecular and crystal structure of native cellulose were established in 1974 independently by Gardner - Blackwell and Sarko - Muggli, who used X-ray data recorded on fibres pulled out from Valonia cell wall [1,2]. Since that time, it has been recognized that such cellulose consisted of the superposition of two phases, namely a triclinic one-chain (Ia) and a monoclinic two-chain (Ib) phase [3,4]. There is therefore a necessity to establish a revised molecular and crystal structure corresponding to the two phases of cellulose, using improved experimental diffraction data on highly crystalline samples, but if possible containing pure Ia and pure Ib.

To tackle this problem, we took advantage of a recent method [5] to prepare reconstituted oriented films of cellulose microcrystals resulting from the acid hydrolysis of (i) purified tunicin (Halocynthia roretzi), consisting essentially of Ib cellulose, and (ii) Cladophora sp. consisting of a mixture of Ia and Ib phases. Some of these films were subjected to intra-crystalline deuteration by an hydrothermal treatment in D_2O in the presence of dilute NaOD. This treatment converted all the intra-crystalline OH groups of cellulose into ODs, without affecting the crystallinity and the orientation of the samples. X-ray fibre diffraction diagrams were recorded at room temperature with a wavelength of 0.782Å, using the microfocus beam line ID13 from ESRF. Neutron fibre diffraction diagrams were obtained at room temperature with both the hydrogenated and deuterated samples, using the 4-circle diffractometer D19 at the Institut Laue Langevin operated with a wavelength of 1.3Å. Both neutron and X-ray fibre patterns contained more than one hundred independent reflections up to a resolution of around 1Å. The intensities of the X-ray patterns were substantially different from those obtained with neutrons. In addition with neutrons, the diagrams of the hydrogenated samples differed also markedly from the deuterated ones. Data sets resulting from the analysis of these fibre diagrams were extracted with the use of CCP13 software. The X-ray data were analyzed with linked atom least squares (LALS) methods together with the X-PLOR program. A Fourier difference analysis was also achieved in the neutron data to locate the H/D atoms of the OH/OD. The best resulting models of cellulose Ia and Ib will be presented.

Acknowledgments

Y.N. thanks the French Government and the Japanese

Society for the Promotion of Science for financial support.

References

[1] Gardner, K.H and Blackwell, J., *Biopolymers* (1974) **13**, 1975-2001.
[2] Sarko, A. and Muggli, R., *Macromolecules* (1980) **7**, 486- 494.
[3] Atalla, R.H. and VanderHart, D.L., *Science* (1984) **223**, 283-285.
[4] Sugiyama, J., Vuong, R. and Chanzy, H., *Macromolecules* (1991) **24**, 4168-4175.
[5] Nishiyama, Y., Kuga, S., Wada, M. and Okano, T., *Macromolecules* (1997) **30**, 6395-6397.

Fibrillin X-ray diffraction: studies of an elastic protein

T.J. Wess[1], C.M. Kielty[2] and P.P. Purslow[3]

1 DBMS, University of Stirling.
2 Dept Biological Sciences, University of Manchester.
3 KVL, Copenhagen.

Fibrillin is a long fibrous protein found in the extracellular matrix. It is thought to provide elasticity and also acts as a site for the deposition of elastin in mature tissues. Some anatomical locations however consist entirely of a fibrillin network. Zonular filaments from the mammalian eye contain fibrillin rich microfibrils and no detectable collagen or elastin. These provide an ideal system for the study of the molecular packing of fibrillin microfibrils. X-ray diffraction studies of zonular filaments on beamline 2.1 and 16.1 at the CLRC Daresbury reveal the structure to contain a fundamental axial periodicity of 56nm. This is comparable to the measurements made on isolated microfibrils studied by electron microscopy. X-ray diffraction allows the structure of the microfibrils to be conducted in the fully hydrated state and also under extension. The X-ray diffraction pattern indicates a number of features.

Fibrillin microfibrils give strong first, third and sixth orders of a meridional series. This is interpreted as the presence of a specific axial alignment of fibrillin microfibrils within the fibrillar bundles. In this the adjacent molecules are staggered by one third of the fundamental axial periodicity. The effect of removing Ca^{2+} from the system alters the position and relative intensity of the diffraction series. This is interpreted as the strengthening of the diffraction from the entire population of the microfibrillar bundle. In vitro experiments have indicated that the microfibrillar spacing becomes less variable in the absence of Ca^{2+}. X-ray diffraction of extended tissue samples indicates a change in the fundamental periodicity of the structure. This information has provided a molecular basis for the elasticity of such tissues.

References

[1] Wess, T.J., *et al.*, *FEBS* (1997) **413**, 424-428.
[2] Wess, T.J., *et al.*, *J. Cell Biol.* (1998) **141(3)**, 829-837.

A high-angle neutron fibre diffraction study of the hydration of B-DNA

M.W. Shotton[1], L.H. Pope[1], V.T. Forsyth[1], P. Langan[2], H. Grimm[3], A. Rupprecht[4], R.C. Denny[5] and W. Fuller[1]

1 Physics Department, Keele University, Staffordshire, ST5 5BG, U.K.
2 Institut Laue-Langevin, Avenue des Martyrs, Grenoble, France.
3 Institute for Solid State Physics, Research Centre, Juelich, Germany.
4 Arrhenius Laboratory, Stockholm University, Sweden.
5 Blackett Laboratory, Imperial College, London University, U.K.

A high-angle neutron fibre diffraction study of the hydration of the B conformation of DNA has been performed on instrument D19 at the Institut Laue-Langevin, Grenoble, using a wet-spun sheet sample of DNA. In common with our previous neutron fibre diffraction studies of DNA, this work exploited the ability to isotopically replace H_2O around the DNA by D_2O. However, in contrast to previous studies, the sample exhibited 'double orientation' so that it was possible to record a three dimensional diffraction data set. Fourier synthesis techniques were used in order to image ordered water surrounding the DNA. Two chains of ordered water have been identified in the minor groove of the molecule in positions that are consistent with water bridging of sugar O4 and purine N3 or pyrimidine O2 atoms.

References

1 Shotton, M.W., Pope, L.H., Forsyth, V.T., Langan, P., Grimm, H., Rupprecht, A., Denny R.C. and Fuller, W., *Physica B* (1998) **241-243**, 1166-1168.

2 Shotton, M.W., Pope, L.H., Forsyth, V.T., Denny, R.C., Archer, J., Langan, P., Ye, H. and Boote, C., *J. Appl. Cryst.* (1998) **31**, 758-766.

SAXS/WAXS & GIXD as a Tool to Investigate Thin Films

C. Salou[1], N.J. Terrill[1,2], A.J. Ryan[1,2], J.P.A. Fairclough[1] and I.W. Hamley[3]

1 Dept. of Chemistry, University of Sheffield, Brookhill, Sheffield, S3 7HF.
2 CLRC, Daresbury Laboratory, Warrington, WA4 4AD.
3 School of Chemistry, University of Leeds, Leeds, LS2 9JT.

A block copolymer is formed from two or more incompatible polymer segments. High molecular weight copolymers will generally form a microdomain structure on cooling. The relative volume fraction of each block dictates the morphology of this microdomain.

Commercially available block copolymers such as Polystyrene-Polybutadiene (PS-PB), Polystyrene-Polyisoprene (PS-PI) or Poly(ethylene-propylene)-Polydimethylsiloxane (PEP-PDMS) mainly have classical morphologies, for example lamellar, BCC spheres or hexagonally packed cylinders. Lamellar structures are obtained if the relative volume ratio of the blocks, determined by NMR, is in the order of 0.5.

X-ray scattering and Reflectivity are methods that can be used to investigate the microdomain morphology of block-copolymer thin films that are spun cast on substrates (e.g. silicon wafers). Reflectivity measurements are also useful for the determination of film thickness, and in the case of lamellar morphologies, in layer thickness determination.

1-D High Resolution Structure of Type I Collagen

J.P. O'Dubhthaigh-Orgel, T.J. Wess and A. Miller

University of Stirling

Although the tri-peptide repeat and periodic features of type I collagen are thought to be well understood, it has not yet been possible to produce a calculated structure with meridional intensities that closely match that of the observed data. The conformation of the n and c terminal telopeptides are still to be established, along with several aspects of the lateral organisation of microfibrils. For the purposes of this project, meridional orders have been observed and recorded for native, and heavy atom stained collagen from rat tail tendon beyond 120 orders (previously, the highest published set of intensities included the 52nd order). This data has been used to produce a model independent set of phases (currently using 92 orders) and hence calculated 1-D axial structure of the molecule at approximately 0.73 nm resolution, the highest resolution previously achieved being approximately 1.29 nm. Also, a large number of models have been constructed where the d-stagger repeat of each of the five chains has been altered, and various different contracted and folded telopeptide conformations used to generate calculated intensity sets that were compared to that of the observed data systematically.

Ordered water around deuterated A-DNA by neutron fibre diffraction

L.H. Pope[1], M.W. Shotton[1], V.T. Forsyth[1], P. Langan[2], R.C. Denny[3], U. Giesen[2], M.T. Dauvergne[4] and W. Fuller[1]

1 Physics Department, Keele University, Staffordshire, ST5 5BG, England.
2 Institut Laue Langevin, Avenue des Martyrs, Grenoble, France.
3 Blackett Laboratory, Imperial College, London University, England.
4 EMBL Outstation, Grenoble, France.

A neutron fibre diffraction study of A-DNA hydration has been carried out using instrument D19 at the Institut Laue-Langevin, Grenoble. Deuterated DNA was used in order to minimise incoherent

scattering and sample absorption effects. Fourier analysis of data collected from the sample in a D_2O environment has revealed four distinct major groove ordered water sites. A network of ordered water involved in the bridging of successive O1 phosphate oxygen atoms along the double helix backbone has been identified. Extensive hydration of the major groove base edges has been observed as a continuous core of density running down the helix axis. The other two hydration features are located in the centre of the major groove, one at the opening of the groove and the other located deep in the groove.

References

[1] Shotton, M.W., Pope, L.H., Forsyth, V.T., Langan, P., Denny, R.C., Giesen, U. and Dauvergne, M.T., *Biophysical Chemistry* (1997) **69 (1)**, 85-96.

[2] Pope, L.H., Shotton, M.W., Forsyth, V.T., Langan, P., Denny, R.C., Giesen, U., Dauvergne M.T. and Fuller, W., *Physica B* (1998) **241-243**, 1156-1158.

An Investigation into the Properties of Polyurethane Hot-Melt Adhesives

M.J. Clarke

University of Sheffield, Department of Chemistry.

Reactive hot-melt adhesives (RHM's) are thermoplastic polymers which are applied to the substrate in the molten state. Upon cooling, the adhesive solidifies and subsequently cross-links on reaction with ambient moisture to form a thermosetting polymer with desirable mechanical properties. Manufacturing processes which use RHMs, such as bookbinding, require the rapid build up of adhesive strength so that bonded parts may be set aside in the minimum time. Important in determining the effectiveness of such adhesives is the strength before curing and the mechanism of solidification leading to this "green strength". Mechanisms may include vitrification, crystallisation and microphase separation. In this study, techniques including rheometry, X-ray scattering and optical microscopy have been used to investigate the solidification mechanisms and viscoelastic properties of polyurethane reactive hot-melt adhesives.

8th Annual Fibre Diffraction and Non-Crystalline Diffraction Workshop

15th-17th June 1999

University of St Andrews

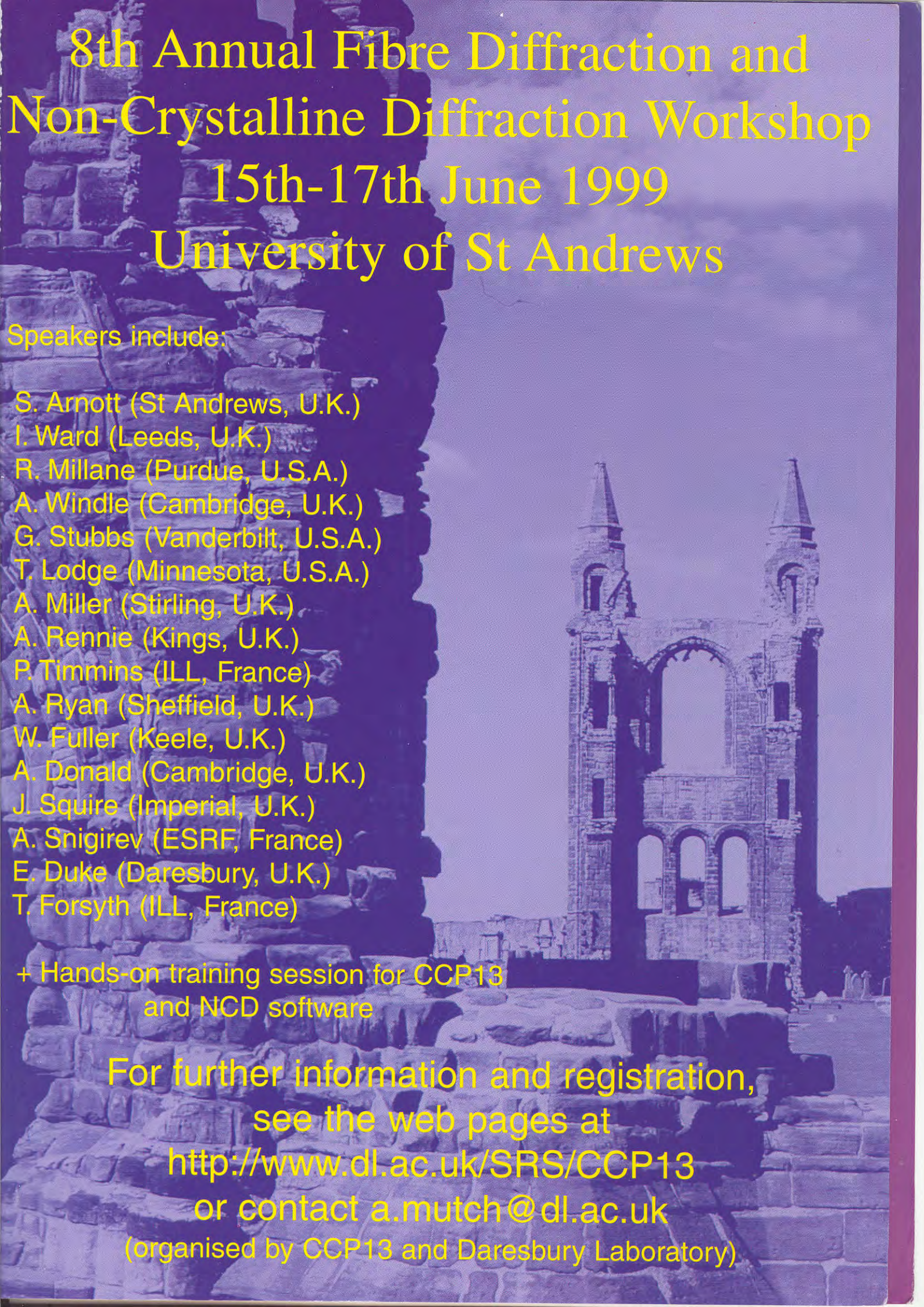

Speakers include:

S. Arnott (St Andrews, U.K.)
I. Ward (Leeds, U.K.)
R. Millane (Purdue, U.S.A.)
A. Windle (Cambridge, U.K.)
G. Stubbs (Vanderbilt, U.S.A.)
T. Lodge (Minnesota, U.S.A.)
A. Miller (Stirling, U.K.)
A. Rennie (Kings, U.K.)
P. Timmins (ILL, France)
A. Ryan (Sheffield, U.K.)
W. Fuller (Keele, U.K.)
A. Donald (Cambridge, U.K.)
J. Squire (Imperial, U.K.)
A. Snigirev (ESRF, France)
E. Duke (Daresbury, U.K.)
T. Forsyth (ILL, France)

+ Hands-on training session for CCP13 and NCD software

For further information and registration, see the web pages at http://www.dl.ac.uk/SRS/CCP13 or contact a.mutch@dl.ac.uk

(organised by CCP13 and Daresbury Laboratory)

Useful World Wide Web addresses (URL)

CCP13	**http://www.dl.ac.uk/SRS/CCP13**
NCD	**http://www.dl.ac.uk/SRS/NCD**
SRS	**http://www.dl.ac.uk/SRS**
DARTS	**http://www.srs.dl.ac.uk/DARTS/index.html**